Spatially precise transfer of patterned monolayer WS_2 and MoS_2 with features larger than 10^4 μm^2 directly from multilayer sources

Hannah M. Gramling,[1] Clarissa M. Towle,[2,3] Sujay B. Desai,[3,4] Haoye Sun,[2] Evan C. Lewis,[1] Vu D. Nguyen[1], Joel W. Ager III,[2,3] Daryl C. Chrzan,[2,3] Eric M. Yeatman,[5] Ali Javey,[3,4] and Hayden K. Taylor[1]*

[1] Department of Mechanical Engineering, University of California, Berkeley, Berkeley, CA 94720, USA

[2] Department of Materials Science and Engineering, University of California, Berkeley, Berkeley, CA 94720, USA

[3] Materials Sciences Division, Lawrence Berkeley National Laboratory, 1 Cyclotron Road, Berkeley, CA 94720, USA

[4] Department of Electrical Engineering and Computer Sciences, University of California, Berkeley, Berkeley, CA 94720, USA

[5] Department of Electrical and Electronic Engineering, Imperial College London, Exhibition Road, London SW7 2AZ, UK

* Correspondence and requests for materials should be addressed to H.K.T. (e-mail: hkt@berkeley.edu).

Abstract

A current challenge in the processing of 2D materials, or 'van der Waals (vdW) solids', is the transfer of 2D layers from source crystals and growth substrates onto target substrates. Transfer—as opposed to direct growth and patterning on the target—enables low-temperature processing of the target as well as the use of diverse target materials. These two attributes will allow the assembly of vdW heterostructures to realize devices exploiting the unique properties of vdW materials. Until now, however, there has been no effective method for transferring regions of monolayer material of controlled shape from a multilayer source. We introduce such a method, and demonstrate its use in the spatially-controlled transfer of arrays of single-layer MoS_2 and WS_2 sheets from multilayer crystals onto SiO_2 substrates. These sheets have lateral sizes exceeding 100 µm and are electronically continuous. The method offers a scalable route to parallel manufacturing of complex circuits and devices from vdW materials.

Introduction

Van der Waals (vdW) solids are composed of single- to few-atom-thick 'two-dimensional' layers loosely bound to each other by van der Waals forces. Their thinness results in extreme mechanical flexibility and exceptional properties, enabling many applications[1] including in electronics[2,3], photonics[4], and chemical sensing[5]. A growing appreciation of the properties of 2D materials has enabled increasingly sophisticated material heterostructures[6,7] and increasingly integrated circuits containing, to date, over 100 2D material-based devices[8]. Interfaces between semiconducting, conducting and insulating 2D materials find applications in, *e.g.*, field-effect transistors (FETs)[9], memristive memories[10], diodes[11], including light-emitting diodes (LEDs)[12,13], photodetectors[12], photovoltaics[14], and catalysis[14].

However, to fabricate multi-material 2D structures through sequential vapor-phase deposition, lithography, and etching steps on a single substrate—as in conventional semiconductor manufacturing—is fraught with difficulties. Firstly, although single-layer vapor-phase deposition techniques such as chemical vapor deposition are now maturing[1,15], the development of processes to deposit one specific 2D material on top of another, while possible[16,17], is time-consuming (*e.g.* 26 hours required[15] for uniform monolayer MoS_2 or WS_2 on SiO_2). Moreover, continuous layers of uniform thickness may prove impractical to produce because of lattice mismatches or chemical incompatibilities. While some fabrication flows actually exploit selective deposition characteristics to form overlap junctions (< 1 µm) at pattern edges[18,19], many applications such as LED displays will demand larger ($\gtrsim 10$ µm) planar junctions between sheets of material. Secondly, when a particular layer of a heterostructure needs to be patterned without destroying those underneath—*e.g.* to enable electrical contact—either extremely high etch selectivity or atomically precise control of etching depth is needed.

These requirements are likely to be impractical to achieve because of difficulties in selecting appropriate etchants and inevitable etch-rate spatial nonuniformities.

Thirdly, the high temperatures of typically 400–1000 °C required for vapor-phase deposition[1,16] impose challenging thermal budgets and preclude the use of polymeric substrates, which are highly desirable for flexible electronics and would truly take advantage of 2D materials' inherent flexibility[9].

Attention has therefore turned to transfer-based assembly methods. Techniques using the surface tension of liquids to maneuver 2D monolayers into position offer limited spatial precision, are prone to wrinkling and folding[20], and introduce residues at the monolayer–substrate interface[1]. Dry transfer (exfoliation) techniques have harnessed normally-applied[21], shearing[22], and mixed-mode[23] mechanical stresses to separate material from naturally-occurring and synthetic sources. Several of these methods provide some within-layer dimensional precision, but layer *thickness* selectivity when exfoliating from multi-layer sources has often been limited (supplementary Fig. S1). Yet atomic monolayers are generally essential, *e.g.* for achieving a direct bandgap in MoS_2[24,25]. What is needed is a technique with precision in all three dimensions, that can handle continuous sheets with lateral dimensions of many tens of micrometers or larger. Such large lateral sheet dimensions are needed for at least two possible purposes: (1) to provide material on which can be created integrated circuits with many sub-micron devices in a pre-defined spatial arrangement; or (2) to define the boundaries of, *e.g.*, powerful individual visible light emitters or sensitive detectors requiring dimensions in the tens of microns or larger. Moreover, a process which simultaneously achieves shape selectivity and monolayer selectivity is desirable for forming arrays of heterostructures, by enabling the

deposition of a patterned monolayer array at the final substrate (which may already have patterned monolayer arrays on its surface).

Recently, the prospects for monolayer exfoliation to be used as a manufacturing process have improved markedly with the discovery that a thin Au film can be used to mediate the single-step exfoliation of large-area monolayers (>10^4 μm^2) from multilayer sources[26,27]. What that work did not achieve was precise control of monolayer shape or position (supplementary Fig. S1), meaning that one was still required to comb over a target substrate for usable material. Recent work leveraging the same principle has demonstrated the transfer of larger-area sheets[28], though subsequent patterning of material deposited on the substrate is necessary to form devices.

The principles underlying this monolayer selectivity have recently started to be understood[29,30]. Essentially, molecular dynamics modeling[30] shows that when a metal is evaporated onto a 2D material crystal, the lattice mismatch between the metal and the 2D material induces a compressive strain in the top layer of the 2D material, weakening the bond between the top and second 2D layers so that a crack preferentially propagates between them when a load is applied (see also supporting Section S2). This crucial phenomenon removes the need for atomically precise etching of 2D materials prior to exfoliation of defined shapes of material. It therefore points towards the development of exfoliation-based transfer of patterned vdW monolayer materials.

The manufacturing process that we introduce (Fig. 1) uses gold-mediated exfoliation in conjunction with a lithographically patterned handle layer to transfer arrays of monolayer regions with controlled shape, size, and separation. Our approach delivers a far higher areal density of usable, continuous monolayer material than unpatterned exfoliation[26,27,29], and does so in

predictable relative locations so that arrays of devices can subsequently be created in a systematic way.

Methods

Overview and novelty

The process for creating patterned monolayers is shown in Fig. 1. It makes use of the recently established gold-mediated monolayer-selective exfoliation phenomenon, but adds a *pre-exfoliation* patterning stage in which photolithography followed by etching (wet etching of the gold, then plasma etching of the 2D material) defines the edges of regions to be exfoliated. What is particularly new and advantageous about this process is that the etching process *does not need to be atomically precise*: rather, the plasma etch creates crack initiation locations at the edges of the desired regions of material, while the deposition of the metal film ensures that those cracks propagate between the first and second layers of the 2D material. What is also demonstrated for the first time is spatial predetermination of where these regions of material are exfoliated. Making blanket contact between a transfer adhesive and a gold-coated 2D crystal—as in previous reports—does, every so often, produce some very large areas (>10^4 μm^2) of monolayer material, but they are ultimately very sparse on the substrate and their locations cannot be predicted. Etching material on the substrate *post-transfer* would not overcome this limitation. Patterning the crystal *before* exfoliation, as we do, initiates cracks that succeed in dictating where material will be exfoliated. Our new method thus generates arrays of monolayer regions with controlled shape and relative position.

Even moderate yield of successfully transferred monolayer regions within such an array is useful, because the user of that material no longer needs laboriously to seek individual

monolayer regions on which to create devices. Instead, it is simply necessary to image each location in the known array, determine which have yielded monolayer material, and systematically use those locations for devices. These steps can in principle readily be automated and are compatible, for example, with the use of lithography masks carrying large arrays of device electrodes to be superimposed on the transferred 2D material. In this work we show yields of monolayer features above 50% in some transferred arrays (see results, esp. Table S1): while not yet nearing semiconductor industry production-level yields, such values are more than enough to accelerate device development greatly compared to the use of unstructured exfoliation.

Moreover, our process itself is rapid compared to state-of-the-art monolayer CVD processes, which require, *e.g.*, 26 hours' growth[15] even before transfer and patterning. Our process, which results in fully patterned monolayers on a target substrate, requires fewer than 10 hours, before any automation. The most time-costly steps are the evaporation (~45 minutes are required for vacuum pump-down), the photolithographic patterning (~1 hour), and the acetone rinse (4 hours). Key aspects of the process design are described below, followed by full, step-by-step details of the process.

Mechanical design of the photoresist handle

A further innovative aspect of the process is that the thickness of the photoresist handle is chosen based on contact mechanics modeling (supplementary Section S3) so that when thermal-release tape is attached to the top surface of the handle pattern prior to exfoliation, the ~300 kPa pressure needed to trigger adhesion does not deform the tape enough to touch the source material between the features. In this way, exfoliation occurs only within the desired features. The required handle thickness depends on the elastic modulus of the thermal-release tape as well as the geometries of the features to be exfoliated, and particularly on their spacing. In the results

presented here, arrays of 320 µm × 40 µm features separated by 120 µm are found to need a handle thickness of at least 12 µm, which is readily obtained with spun-on commercial photoresists.

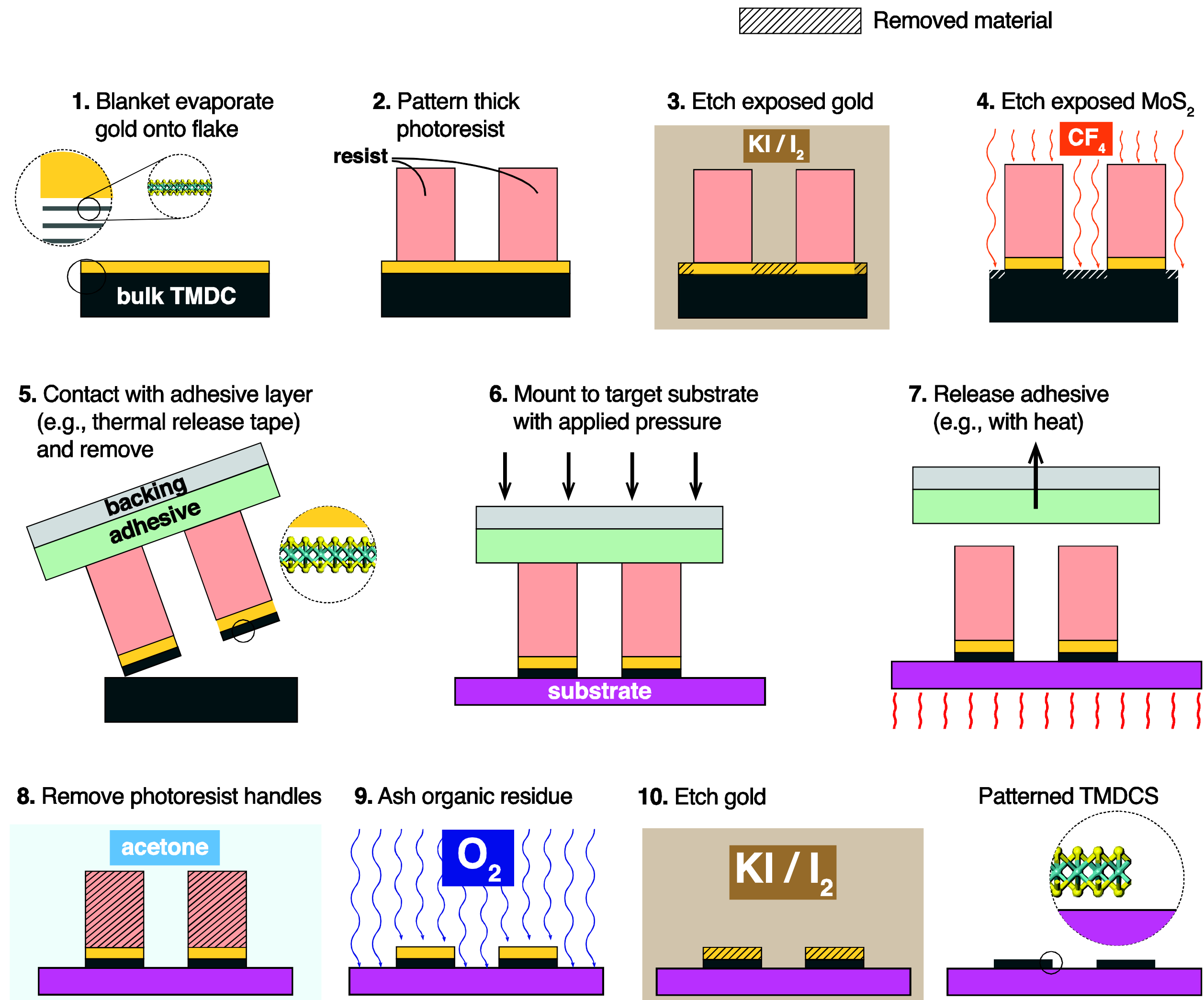

Figure 1 | Process for producing patterned monolayers. The process for patterning and transferring van der Waals monolayers uses standard photolithography techniques. It relies on the use of a thick handle layer (here, photoresist, step 2) to pattern the gold and the underlying layered bulk material, as well as to offset the adhesive transfer medium from the bulk, thus permitting transfer of only the patterned regions.

Transfer of material

After exfoliation from the source, the material is transferred via the thermal release tape to the target substrate (SiO_2 in this work), heat and pressure are applied, the tape and photoresist are stripped away, and the remaining gold is etched. This process ensures that the interface between the exfoliated material and the target substrate remains dry and never touches any other materials. Moreover, the gold layer prevents direct contact between the transferred monolayer and any organic solids. These attributes are expected to minimize heterostructure contamination.

Detailed process steps

1. The multilayer source material (in this work, MoS_2 or WS_2) is prepared. The flattest available sections of material are used. In the case of MoS_2, natural, mined crystals were obtained (eBay) and were manually cleaved to create a flake several mm in diameter and a fraction of a millimeter thick. This flake was mounted to a glass slide using double-sided Kapton tape for subsequent processing. Both WS_2 and additional MoS_2 samples were obtained as a multi-layer sample fabricated by chemical vapor transport (CVT), ~0.2–0.3 mm thick (HQ Graphene) and used as received. The prepared source material is coated with a 100 nm-thick layer of gold by thermal evaporation (Torr International, Inc.).
2. The source material is coated with AZ 4620 photoresist (PR, MicroChemicals GmbH) which is then patterned (details in supporting Section S8: Photolithography).
3. Without removing the photoresist layer, the exposed gold is etched for 1 minute in KI/I_2 (Gold Etchant TFA, Transene Company, Inc.; used undiluted). This step exposes the MoS_2 or WS_2 that is not to be transferred, while the to-be-transferred material remains masked by gold and photoresist. The sample is rinsed in DI water.

4. The patterned flake is then exposed to a 30-second etch in CF_4 plasma (20 sccm, 100 W, Plasma Equipment Technical Services, Inc.) to remove at least one atomic layer of the MoS_2 or WS_2 from unmasked regions. Initially, a one minute etch time was used to ensure the removal of at least the top layer[31]; however, the longer etch time was correlated with large amounts of organic residue on the sample, and was adjusted down. As an alternative to a plasma etch, an argon ion milling step may be used. Ion milling (Pi Scientific 6" system) was conducted using Argon ion (5 sccm RF neutral, 15 sccm ion source), with 100 mA beam current, 500 V beam voltage and 20 degree incidence angle. The duration of the mill was 7 minutes and the pressure was 1.9×10^{-4} Torr. In some cases it was found that the photoresist was easier to remove in step (8) below when ion milling had been used than when the CF_4 etch had been used, possibly because of fluoropolymer deposition onto the photoresist during CF_4 processing. The results shown in this paper, however, were all obtained with CF_4 etching.[*]
5. Thermal release tape (REVALPHA, Nitto) is brought into contact with the remaining photoresist pattern. Light manual pressure is applied by brushing rubber-tipped tweezers against the back side of the tape, and the tape, loaded now with the pattern, is peeled by hand from the bulk flake.[†]
6. The silicon wafer target substrate with 260 nm silicon oxide is treated in O_2 plasma for 5 minutes (120 W, Diener Electronic Nano). It is then placed on a hot plate at 80 ºC for at least

[*] Although the etching or ion milling process does change the topography of the source material left behind after exfoliation, the source crystal can be re-used, if there are enough layers remaining, by doing a blanket exfoliation with unpatterned thermal release tape to recover a close-to-flat surface.

[†] If a transparent transfer medium were chosen, such as the elastomer polydimethylsiloxane (PDMS), the technique would be compatible with optical alignment methods which would allow placement of sheets in controlled positions on a target.

five minutes, and an IR gun is used to verify it has reached 80 ºC.‡ The tape, loaded with the patterned material, is placed onto the heated target substrate and pressure is applied to the tape/substrate stack for 5 minutes using a 6.8 kg weight atop a rubber stopper (area: 11 cm^2, thickness: 2.54 cm (1”)). The purpose of the rubber is to distribute the load uniformly over the uneven micro-topography of the patterned tape’s surface. The applied pressure is approximately 60 kPa.

7. The target substrate, carrying the loaded tape, is moved to a hot plate at 160 ºC to trigger the release of the thermal tape.
8. The transferred stack is now adhered to the silicon/silicon oxide substrate and is placed in acetone for at least four hours to remove the photoresist.
9. The substrate is ashed in O_2 plasma (3 minutes, 20 sccm, 300 W, Plasma Equipment Technical Services, Inc.) to remove any organic residue on the surface. During the ashing step, the remaining gold layer protects underlying MoS_2 or WS_2 monolayers from damage or removal.
10. Finally, the remaining gold is stripped in KI/I_2 and the sample is rinsed in DI water. The result is monolayer TMDC material on the silicon/silicon oxide substrate (**Fig. S13**).

Results and discussion

The technique is demonstrated using chemical-vapor-transport-grown bulk WS_2 (Fig. 2) as well as mined crystals of naturally occurring MoS_2 (supplementary Fig. S4) as sources. Results of the transfer process have been examined with optical microscopy, photoluminescence (PL)

‡ The use of oxygen plasma and elevated temperature has previously been shown[32] to enhance adhesion of exfoliated 2D materials to SiO_x and thereby greatly increase the transferred area of material, albeit, in that work, without control of shape or position.

imaging and spectroscopy, and characterization as a FET channel (all methods in supplementary material).

Optical characterization of transferred material

Monolayer regions within an array of ≳100 transferred WS_2 features are identified from white-light optical reflection micrographs using well-established optical contrast methods[33,34] (Fig. 2a). These micrographs show that features printed using the method are predominantly composed of monolayer material and include substantial continuous monolayer areas. The monolayer nature of these regions is confirmed with PL imaging[24,25] (Fig. 2b for WS_2 and Fig. S4 for MoS_2). While the PL intensity of monolayer regions shows some feature-to-feature and within-feature variation, all regions with appreciable intensity in the PL images indicate monolayer material, because the emitted PL intensity of a monolayer is at least two orders of magnitude larger than that of bilayer or multilayer material[24,35]. Spatial nonuniformity of PL intensity could be attributable to spatial variation of the density of sulfide vacancies—vacancies which can be repaired by a superacid treatment[26] as we describe below.

Meanwhile, the measured PL peak energies of representative monolayer regions show sample standard deviations of 21 meV for WS_2 (13 measurement locations; Fig. 2c) and 6 meV for MoS_2 (10 measurement locations; supplementary Fig. S4c), which may indicate modest spatial variation of the material's environment, such as from processing residue, sulfide vacancies, or strain state[36]. Raman spectroscopy (supporting section S5 and Figs. S5–S6 and S8) further confirms the single-layer nature of regions that had already been identified as such by both optical reflectance and PL.

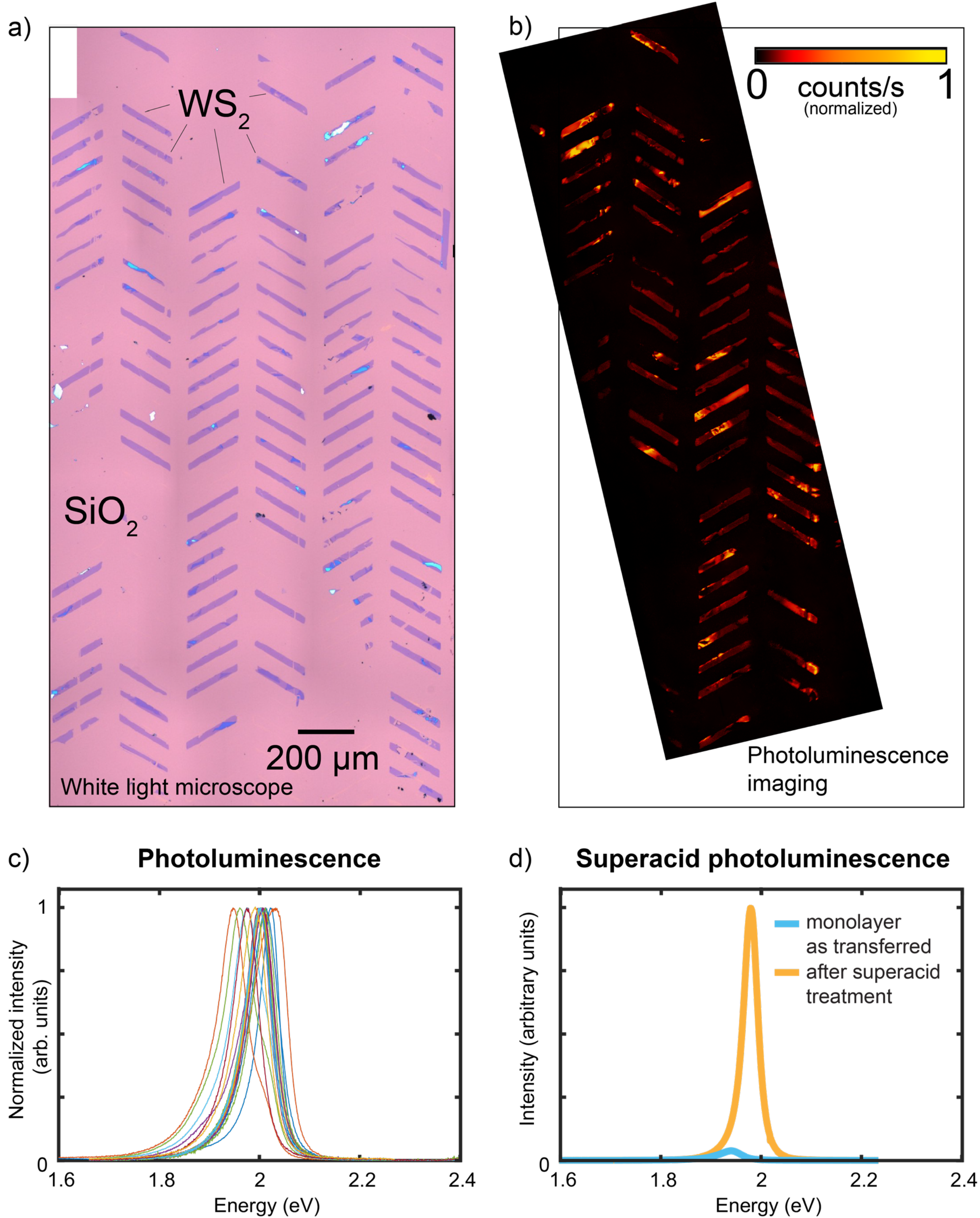

Figure 2 | Optical and optoelectronic WS_2 monolayer characterization. (a) White-light reflectance image of a set of transferred WS_2 features on 260 nm thermal SiO_2 on Si; (b) photoluminescence image of part of the same region as in (a): orientation is the same as (a), and the outline corresponds to that of the region imaged in (a); (c) photoluminescence spectra from 13 regions of WS_2 on 260 nm thermal SiO_2 on Si, confirming that monolayer WS_2 has been transferred to the substrate; (d) the result of treating a WS_2 monolayer with a superacid, showing more than a twenty five-fold increase in quantum efficiency.

Feature and areal yield of the process

Fig. 3 shows histograms summarizing the surface areas of regions of continuous monolayer material on three WS_2 and three MoS_2 samples. Details of how the histograms were constructed from optical reflation images are given in supporting Section S7. These results show that the process is capable of depositing monolayer sheets of both materials with areas larger than 10^4 μm^2. Moreover, the *average* areas of monolayer sheets are considerably higher than those obtained with unpatterned gold-mediated exfoliation[26] in all but one case (Fig 3e). We further emphasize that each histogram in Fig. 3 is obtained from *one single exfoliation process* onto a single substrate, whereas the distributions characterizing unpatterned exfoliation were accumulated from many samples, with material occurring more sparsely over far larger total substrate areas[26].

We characterize the yield of the process using two metrics: *feature yield* and *areal yield* (details in supporting Section S7). Feature yield refers to the number of features actually transferred as a fraction of the total number of desired features in a given area. Areal yield measures the area of monolayer material in a given feature, as a fraction of the total intended feature area. Both metrics are potentially relevant for device integration. Areal yield is assessed with a custom image processing routine, by determining the areas of any monolayer regions in each feature, and dividing the monolayer area by the desired area of the feature. Feature yield ranges up to 67% for WS_2 and up to 54% for MoS_2 (supplementary Table S1). Mean areal yields of 63% for WS_2 and 55% for MoS_2 are obtained. While these values remain, of course, below those typical in mainstream semiconductor manufacturing, they represent exceptionally high levels in the current context of exfoliated vdW material processing, and can thus accelerate experimental progress in the field by reducing time spent isolating monolayers.

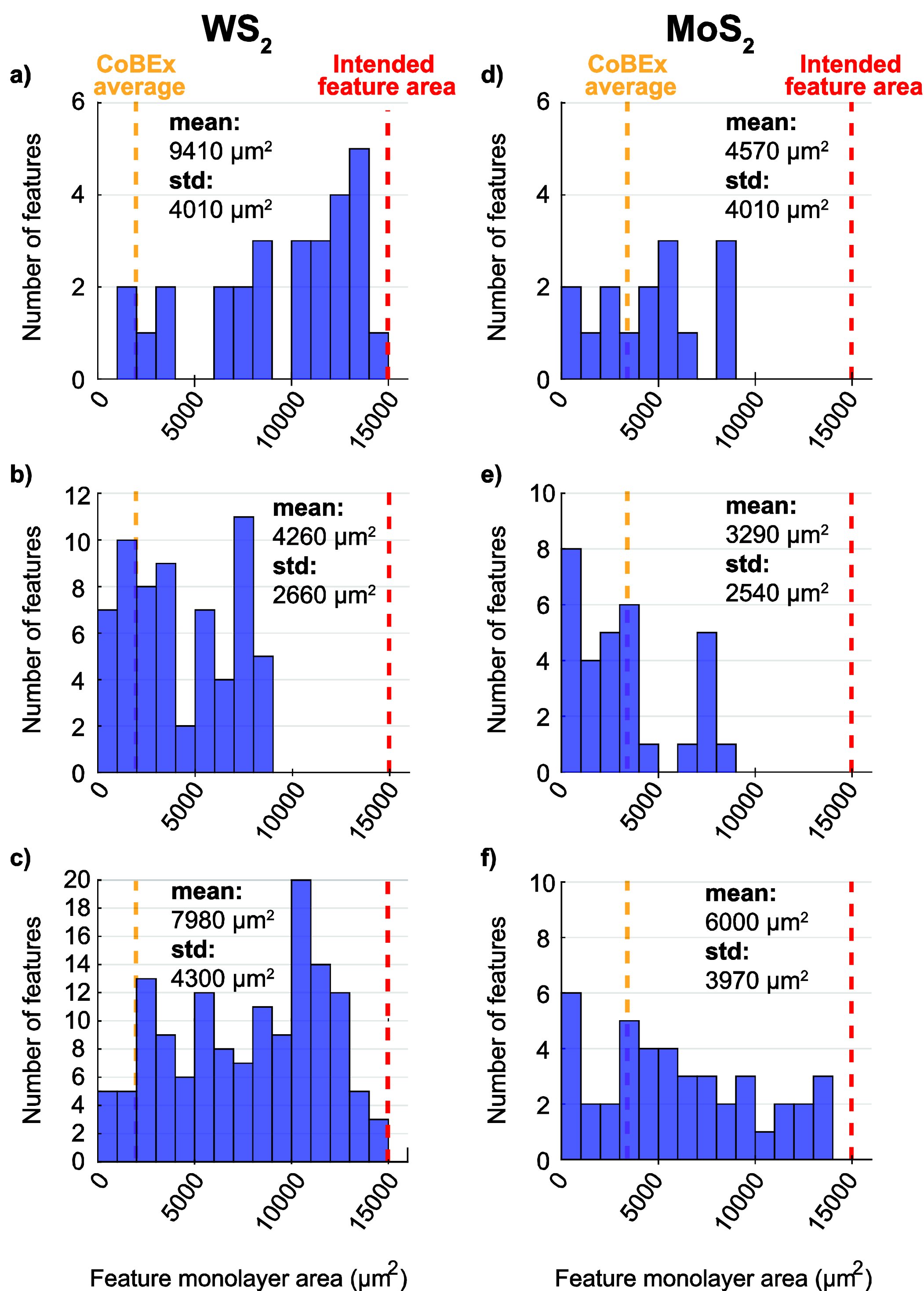

Figure 3 | Yield results of the exfoliation method. Histograms (blue bars) showing the distributions of the areas of regions of continuous monolayer material transferred to three separate substrates patterned with WS_2 (a–c) and three substrates patterned with MoS_2 (d–f). Samples were all created using the process flow of Fig 1, with the exfoliated material being the only variable. The red dashed line indicates the area that would be occupied in a pattern by a full, perfect feature; the yellow dashed line shows the average area of continuous material obtained from many samples using the prior, unpatterned, gold-mediated 'CoBEx' method[26].

Sources of yield loss

We have identified three processing steps that contribute most significantly to yield loss, and that would therefore be a reasonable focus of future process development. Firstly, in step 5 (as defined in 'Detailed process steps' above), some of the patterned photoresist handles do not adhere to the thermal release tape and therefore remain on the source crystal. This source of defectivity is evident from optical examination of the thermal release tape between steps 5 and 6, in which gaps are visible in the array of features on the tape. Strengthening binding between the PR handles and the adhesive film would help to address this issue, *e.g.* by applying a partially baked PR layer to the tape.

Secondly, in some features, the photoresist–gold bond fails during step 5 and the gold and 2D layer therefore remain on the source crystal even when the photoresist feature is transferred to the tape. This source of defectivity is again evident from optical examination of the thermal release tape immediately after step 5, in which some of the photoresist features are visible but without the highly reflective gold layer on them. To address this source of yield loss, adhesion of the photoresist to the gold should be enhanced, potentially by adding an O_2 plasma or hexamethyldisilazane (HMDS) treatment between steps 1 and 2, although this has not yet been tried.

Thirdly, in some locations where gold polygons are visible on the substrate after step 9, optical reflectance imaging after step 10 shows that the MoS_2 or WS_2 is ultimately absent from those same locations. We attribute this component of yield loss to ingress of KI/I_2 liquid between the 2D layer and the substrate during the gold etch of step 10, washing the 2D material off the substrate. This explanation is more plausible than earlier failure of the gold–2D material interface, since that interface is formed during the gold evaporation and is known to be strong

because of the Au–S bond. We found that limiting the time that elapses between step 9 (exposing the substrate and its contents to O_2 plasma) and step 10 (gold KI/I_2 processing) to below an hour greatly mitigates this third yield limitation, resulting in the yield values reported above and in Table S1. Nevertheless, further refining this apparently critical plasma treatment step and/or thermally annealing the substrate before the final gold etch may be beneficial in improving the yield of step 10 beyond the values presently reported.

Photoluminenscence enhancement by superacid treatment

Representative samples were further treated in bis(trifluoromethane) sulfonimide (TFSI) superacid (details in supplementary Section S4) to determine whether this method could improve the quantum yield of the monolayer material, as has been demonstrated previously with unstructured exfoliation[26]. Large observed increases of PL intensity in response to equal illumination after superacid treatment (Fig. 2(d) for WS_2 and supplementary Fig. S4(d) for MoS_2) show that indeed the superacid treatment increases the quantum yield at least 25 times in the case of WS_2, and at least 100 times in the case of MoS_2.

Electrical characterization

Back-gated FETs with gate lengths of 10 μm were defined using photolithographically patterned nickel source and drain electrodes, laid on top of transferred MoS_2 and WS_2 monolayer regions (Fig. 4; processing details are in supplementary Section S6). Devices were then randomly selected for electrical testing from among those whose *entire channel region* had been optically confirmed to consist of monolayer material. In the case of MoS_2, 20 monolayer devices across two substrates were selected for testing; in the case of WS_2, six monolayer devices were sampled from one substrate. The I_D–V_{GS} characteristics of all tested MoS_2 and WS_2 devices are shown in Fig. S7 and Fig. S8 respectively.

It is notable that all 20 of the 20 tested MoS_2 devices functioned as FETs, exhibiting strong switching behavior with on/off current ratios at V_{DS} = 1 V of between 10^3 and 10^7. Meanwhile, four of the six WS_2 devices tested showed unambiguous switching behavior at V_{DS} = 1 V, with on/off current ratios between ~200 and 10^4. These results suggest that the transferred material predominantly retains its semiconducting performance and electrical continuity, with the evidence being especially strong for the MoS_2.

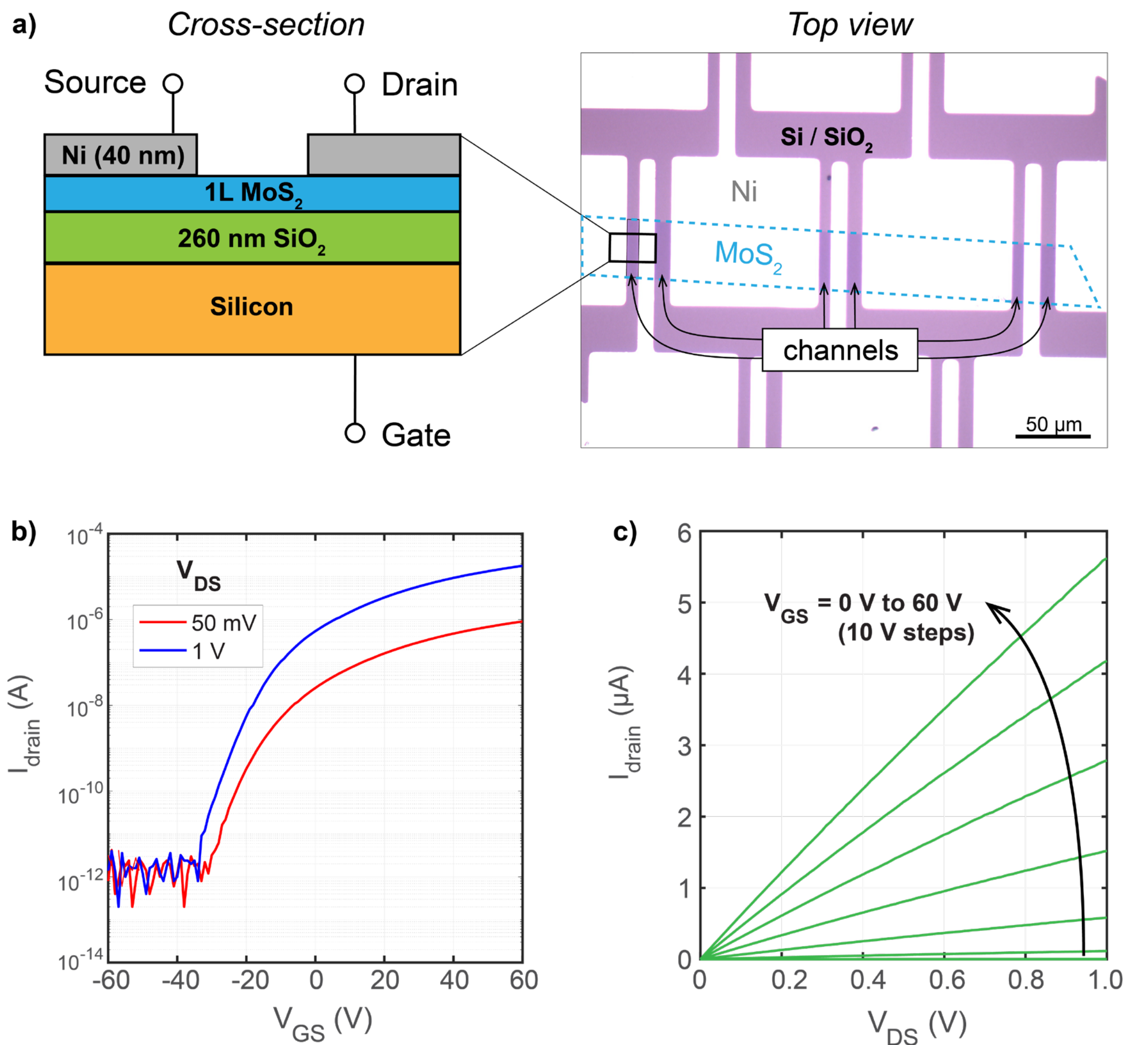

Figure 4 | Device characteristics. a) Cross-section and optical micrograph of six fabricated back-gated MoS_2 transistors with channel width up to 40 μm, defined by the patterning process, and a gate length of 10 μm defined by the Ni contacts. b) Switching behavior of one of the devices fabricated from transferred monolayer MoS_2 material. c) Drain current as a function of drain–source voltage.

Atomic force microscopy and surface residues

Atomic force microscopy (AFM) measurements of transferred material were also performed (supplementary Figs. S9–S11 and Section S9). While the optical reflection, PL and Raman measurements described above provide ample robust evidence of the presence of monolayer material, the AFM measurements offer additional information about the topography of transferred material. We see from the AFM topographies that there is some evidence of particle-like residues on both the transferred material and substrate after processing is complete. These residues are approximately 5 nm tall, and XPS analysis (supplementary Section S10 and Fig. S11a) suggests that they are composed of gold.

Our FET device characterization measurements have confirmed that our test devices, which have 10 μm channel lengths, exhibit strong switching behavior. The residues are therefore evidently sparse enough not to inhibit operation of devices at the 10 μm length-scale. Since our XPS analysis of the residue indicates that it is gold, it is conceivable that as devices are scaled down, the residue might provide a current-shorting path, but such behavior has not been observed.

Another potential concern might be that surface residues could inhibit the formation of planar heterostructures requiring atomically-spaced layers. To examine this possibility we formed a planar interface between two MoS_2 monolayers that were transferred sequentially using our process followed by thermal annealing (details in supporting information, Section S9 and Fig. S12). The Raman spectra measured at multiple locations on this constructed bilayer are consistent with bilayer material—and *not* with two separate monolayers—which indicates that the layers became atomically close after transfer and annealing. Such behavior indicates that whatever residues were on top of the first-deposited MoS_2 layer did not inhibit the formation of

intimate contact between it and the second-deposited MoS_2 layer. It is probable that the residues are so sparse that a monolayer of a 2D material can easily conform to them.

The XPS evidence that these residues are gold suggests that they could be removed, if necessary, by modification of the final gold etching step, *i.e.* step 10 of the process. Extended KI/I_2 acid treatment of the surface, possibly coupled with one or more of mechanical agitation, sonication, and an extended or more vigorous water or solvent rinsing protocol could assist in residue removal. Certainly for the use of this process in combination with traditional silicon electronics, any gold residue would need to be very thoroughly removed, but for novel circuit integration based entirely on 2D materials, it is not yet known how much of an issue Au contamination may be.

Concluding remarks

What this new processing method essentially achieves is to control where interlayer fracture initiates in vdW solids. It is more effective than simply blanketing the source material with gold because in that case there is no control of where inter-layer fracture events will initiate, and we expect that exfoliated material edges would then correspond to naturally occurring steps in the crystal structure. By introducing etched steps in the material at the edges of the photoresist handles, we can predetermine, at least to an extent, the locations of fracture.

We expect that a key to increasing yield will be to address the three particular defect-inducing process steps discussed above. An additional likely source of defectivity that cannot be attributed to a specific process step is the intersection of patterned gold regions with natural step changes in the height of the source material. These intersections provide opportunities for

patterned handles to contact multiple layers and thereby exfoliate multilayer material. Such intersections could be reduced by maximizing grain size relative to the exfoliated feature size.

This significant step forward in 3D spatial control over exfoliation has been demonstrated here for both MoS_2 and WS_2, and in the future could enable complex integrated circuits to be fabricated more easily from 2D materials. The technique's ability to transfer monolayer sheets with areas $>10^4$ μm^2 makes it particularly appealing for the production of complex heterostructure-based circuits. We have emphasized the capability for large-area transfer although, in principle, there is no impediment to using the technique to transfer arrays of much smaller regions of material, *e.g.* to define many individual sub-micron transistor geometries prior to exfoliation and transfer. The challenge in that case would be to ensure a high enough feature yield to be able to construct the desired integrated circuit without missing devices. In contrast, higher functional yields may be achieved by transferring arrays of large monolayer sheets, as demonstrated, and then defining, *e.g.*, conductive interconnect patterns to create one or more whole integrated circuits within each successfully transferred large monolayer region.

Although the present process exploits Au–S binding to achieve monolayer selectivity[37], the basic mechanism, which hinges on a lattice constant mismatch, is expected to be applicable to other material pairs (see supplementary Section S2), and would be a valuable focus of future studies. Additionally, metal-mediated exfoliation may find itself used in conjunction with other emerging techniques for epitaxy and transfer of thin films[16,17,38,39] to create semiconductor heterostructures.

References

(1) Li, J.; Östling, M. Scalable Fabrication of 2D Semiconducting Crystals for Future Electronics. *Electronics* **2015**, *4* (4), 1033–1061. https://doi.org/10.3390/electronics4041033.

(2) Das, S.; Gulotty, R.; Sumant, A. V.; Roelofs, A. All Two-Dimensional, Flexible, Transparent, and Thinnest Thin Film Transistor. *Nano Lett.* **2014**, *14* (5), 2861–2866. https://doi.org/10.1021/nl5009037.

(3) Ghatak, S.; Pal, A. N.; Ghosh, A. Nature of Electronic States in Atomically Thin MoS2 Field-Effect Transistors. *ACS Nano* **2011**, *5* (10), 7707–7712. https://doi.org/10.1021/nn202852j.

(4) Yin, X.; Ye, Z.; Chenet, D. a; Ye, Y.; O'Brien, K.; Hone, J. C.; Zhang, X. Edge Nonlinear Optics on a MoS2 Atomic Monolayer. *Science* **2014**, *344* (6183), 488–490. https://doi.org/10.1126/science.1250564.

(5) Perkins, F. K.; Friedman, A. L.; Cobas, E.; Campbell, P. M.; Jernigan, G. G.; Jonker, B. T. Chemical Vapor Sensing with Monolayer MoS_2. *Nano Lett.* **2013**, *13* (2), 668–673. https://doi.org/10.1021/nl3043079.

(6) Geim, A. K.; Grigorieva, I. V. Van Der Waals Heterostructures. *Nature* **2013**, *499* (7459), 419–425. https://doi.org/10.1038/nature12385.

(7) Butler, S. Z.; Hollen, S. M.; Cao, L.; Cui, Y.; Gupta, J. a.; Gutiérrez, H. R.; Heinz, T. F.; Hong, S. S.; Huang, J.; Ismach, A. F.; et al. Progress, Challenges, and Opportunities in Two-Dimensional Materials beyond Graphene. *ACS Nano* **2013**, *7* (4), 2898–2926. https://doi.org/10.1021/nn400280c.

(8) Wachter, S.; Polyushkin, D. K.; Bethge, O.; Mueller, T. A Microprocessor Based on a Two-Dimensional Semiconductor. *Nat. Commun.* **2017**, *8*, 14948. https://doi.org/10.1038/ncomms14948.

(9) Lee, G.-H.; Yu, Y.-J.; Cui, X.; Petrone, N.; Lee, C.-H.; Choi, M. S.; Lee, D.-Y.; Lee, C.; Yoo, W. J.; Watanabe, K.; et al. Flexible and Transparent MoS2 Field-Effect Transistors on Hexagonal Boron Nitride-Graphene Heterostructures. *ACS Nano* **2013**, *7* (9), 7931–7936. https://doi.org/10.1021/nn402954e.

(10) Ge, R.; Wu, X.; Kim, M.; Chou, H.; Sonde, S.; Tao, L.; Lee, J. C.; Akinwande, D. Towards Universal Non-Volatile Resistance Switching in Non-Metallic Monolayer Atomic Sheets. *ArXiv170904592 Cond-Mat* **2017**.

(11) Deng, Y.; Luo, Z.; Conrad, N. J.; Liu, H.; Gong, Y.; Najmaei, S.; Ajayan, P. M.; Lou, J.; Xu, X.; Ye, P. D. Black Phosphorus–Monolayer MoS2 van Der Waals Heterojunction p–n Diode. *ACS Nano* **2014**, *8* (8), 8292–8299. https://doi.org/10.1021/nn5027388.

(12) Bie, Y.-Q.; Grosso, G.; Heuck, M.; Furchi, M. M.; Cao, Y.; Zheng, J.; Bunandar, D.; Navarro-Moratalla, E.; Zhou, L.; Efetov, D. K.; et al. A $MoTe_2$-Based Light-Emitting Diode and Photodetector for Silicon Photonic Integrated Circuits. *Nat. Nanotechnol.* **2017**, nnano.2017.209. https://doi.org/10.1038/nnano.2017.209.

(13) Withers, F.; Del Pozo-Zamudio, O.; Mishchenko, A.; Rooney, A. P.; Gholinia, A.; Watanabe, K.; Taniguchi, T.; Haigh, S. J.; Geim, A. K.; Tartakovskii, A. I.; et al. Light-Emitting Diodes by Band-Structure Engineering in van Der Waals Heterostructures. *Nat. Mater.* **2015**, *14* (3), 301–306. https://doi.org/10.1038/nmat4205.

(14) Li, H.; Shi, Y.; Chiu, M.-H.; Li, L.-J. Emerging Energy Applications of Two-Dimensional Layered Transition Metal Dichalcogenides. *Nano Energy* **2015**, *18*, 293–305. https://doi.org/10.1016/j.nanoen.2015.10.023.

(15) Kang, K.; Xie, S.; Huang, L.; Han, Y.; Huang, P. Y.; Mak, K. F.; Kim, C.-J.; Muller, D.; Park, J. High-Mobility Three-Atom-Thick Semiconducting Films with Wafer-Scale Homogeneity. *Nature* **2015**, *520* (7549), 656–660. https://doi.org/10.1038/nature14417.

(16) Shi, Y.; Zhou, W.; Lu, A.-Y.; Fang, W.; Lee, Y.-H.; Hsu, A. L.; Kim, S. M.; Kim, K. K.; Yang, H. Y.; Li, L.-J.; et al. Van Der Waals Epitaxy of MoS_2 Layers Using Graphene As Growth Templates. *Nano Lett.* **2012**, *12* (6), 2784–2791. https://doi.org/10.1021/nl204562j.

(17) Yu, H.; Yang, Z.; Du, L.; Zhang, J.; Shi, J.; Chen, W.; Chen, P.; Liao, M.; Zhao, J.; Meng, J.; et al. Precisely Aligned Monolayer MoS2 Epitaxially Grown on H-BN Basal Plane. *Small* **2017**, *13* (7), n/a-n/a. https://doi.org/10.1002/smll.201603005.

(18) Zhao, M.; Ye, Y.; Han, Y.; Xia, Y.; Zhu, H.; Wang, S.; Wang, Y.; Muller, D. A.; Zhang, X. Large-Scale Chemical Assembly of Atomically Thin Transistors and Circuits. *Nat. Nanotechnol.* **2016**, *11* (11), 954–959. https://doi.org/10.1038/nnano.2016.115.

(19) Ling, X.; Lin, Y.; Ma, Q.; Wang, Z.; Song, Y.; Yu, L.; Huang, S.; Fang, W.; Zhang, X.; Hsu, A. L.; et al. Parallel Stitching of 2D Materials. *Adv. Mater.* **2016**, *28* (12), 2322–2329. https://doi.org/10.1002/adma.201505070.

(20) Hallam, T.; Shakouri, A.; Poliani, E.; Rooney, A. P.; Ivanov, I.; Potie, A.; Taylor, H. K.; Bonn, M.; Turchinovich, D.; Haigh, S. J.; et al. Controlled Folding of Graphene: GraFold Printing. *Nano Lett.* **2015**, *15* (2), 857–863. https://doi.org/10.1021/nl503460p.

(21) Nam, H.; Wi, S.; Rokni, H.; Chen, M.; Priessnitz, G.; Lu, W.; Liang, X. MoS2 Transistors Fabricated via Plasma-Assisted Nanoprinting of Few-Layer MoS2 Flakes into Large-Area Arrays. *ACS Nano* **2013**, *7* (7), 5870–5881. https://doi.org/10.1021/nn401093u.

(22) Chen, M.; Nam, H.; Rokni, H.; Wi, S.; Yoon, J. S.; Chen, P.; Kurabayashi, K.; Lu, W.; Liang, X. Nanoimprint-Assisted Shear Exfoliation (NASE) for Producing Multilayer MoS2 Structures as Field-Effect Transistor Channel Arrays. *ACS Nano* **2015**, *9* (9), 8773–8785. https://doi.org/10.1021/acsnano.5b01715.

(23) Na, S. R.; Suk, J. W.; Tao, L.; Akinwande, D.; Ruoff, R. S.; Huang, R.; Liechti, K. M. Selective Mechanical Transfer of Graphene from Seed Copper Foil Using Rate Effects. *ACS Nano* **2015**, *9* (2), 1325–1335. https://doi.org/10.1021/nn505178g.

(24) Mak, K. F.; Lee, C.; Hone, J.; Shan, J.; Heinz, T. F. Atomically Thin MoS 2 : A New Direct-Gap Semiconductor. *Phys. Rev. Lett.* **2010**, *105* (13). https://doi.org/10.1103/PhysRevLett.105.136805.

(25) Splendiani, A.; Sun, L.; Zhang, Y.; Li, T.; Kim, J.; Chim, C.-Y.; Galli, G.; Wang, F. Emerging Photoluminescence in Monolayer MoS 2. *Nano Lett.* **2010**, *10* (4), 1271–1275. https://doi.org/10.1021/nl903868w.

(26) Desai, S. B.; Madhvapathy, S. R.; Amani, M.; Kiriya, D.; Hettick, M.; Tosun, M.; Zhou, Y.; Dubey, M.; Ager, J. W.; Chrzan, D.; et al. Gold-Mediated Exfoliation of Ultralarge Optoelectronically-Perfect Monolayers. *Adv. Mater.* **2016**, *28* (21), 4053–4058. https://doi.org/10.1002/adma.201506171.

(27) Magda, G. Z.; Pető, J.; Dobrik, G.; Hwang, C.; Biró, L. P.; Tapasztó, L. Exfoliation of Large-Area Transition Metal Chalcogenide Single Layers. *Sci. Rep.* **2015**, *5* (1). https://doi.org/10.1038/srep14714.

(28) Shim, J.; Bae, S.-H.; Kong, W.; Lee, D.; Qiao, K.; Nezich, D.; Park, Y. J.; Zhao, R.; Sundaram, S.; Li, X.; et al. Controlled Crack Propagation for Atomic Precision Handling of Wafer-Scale Two-Dimensional Materials. *Science* **2018**, eaat8126. https://doi.org/10.1126/science.aat8126.

(29) Velický, M.; Donnelly, G. E.; Hendren, W. R.; McFarland, S.; Scullion, D.; DeBenedetti, W. J. I.; Correa, G. C.; Han, Y.; Wain, A. J.; Hines, M. A.; et al. Mechanism of Gold-Assisted Exfoliation of Centimeter-Sized Transition-Metal Dichalcogenide Monolayers. *ACS Nano* **2018**. https://doi.org/10.1021/acsnano.8b06101.

(30) Sun, H.; Sirott, E. W.; Mastandrea, J.; Gramling, H. M.; Zhou, Y.; Poschmann, M.; Taylor, H. K.; Ager, J. W.; Chrzan, D. C. Theory of Thin-Film-Mediated Exfoliation of van Der Waals Bonded Layered Materials. *Phys. Rev. Mater.* **2018**, *2* (9), 094004. https://doi.org/10.1103/PhysRevMaterials.2.094004.

(31) Jeon, M. H.; Ahn, C.; Kim, H.; Kim, K. N.; LiN, T. Z.; Qin, H.; Kim, Y.; Sehan Lee; Kim, T.; Yeom, G. Y. Controlled MoS 2 Layer Etching Using CF 4 Plasma. *Nanotechnology* **2015**, *26* (35), 355706. https://doi.org/10.1088/0957-4484/26/35/355706.

(32) Huang, Y.; Sutter, E.; Shi, N. N.; Zheng, J.; Yang, T.; Englund, D.; Gao, H.-J.; Sutter, P. Reliable Exfoliation of Large-Area High-Quality Flakes of Graphene and Other Two-Dimensional Materials. *ACS Nano* **2015**, *9* (11), 10612–10620. https://doi.org/10.1021/acsnano.5b04258.

(33) Castellanos-Gomez, A.; Agraït, N.; Rubio-Bollinger, G. Optical Identification of Atomically Thin Dichalcogenide Crystals. *Appl. Phys. Lett.* **2010**, *96* (21), 213116. https://doi.org/10.1063/1.3442495.

(34) Li, H.; Wu, J.; Huang, X.; Lu, G.; Yang, J.; Lu, X.; Xiong, Q.; Zhang, H. Rapid and Reliable Thickness Identification of Two-Dimensional Nanosheets Using Optical Microscopy. *ACS Nano* **2013**, *7* (11), 10344–10353. https://doi.org/10.1021/nn4047474.

(35) Zhao, W.; Ghorannevis, Z.; Chu, L.; Toh, M.; Kloc, C.; Tan, P.-H.; Eda, G. Evolution of Electronic Structure in Atomically Thin Sheets of WS $_2$ and WSe $_2$. *ACS Nano* **2013**, *7* (1), 791–797. https://doi.org/10.1021/nn305275h.

(36) Conley, H. J.; Wang, B.; Ziegler, J. I.; Haglund, R. F.; Pantelides, S. T.; Bolotin, K. I. Bandgap Engineering of Strained Monolayer and Bilayer MoS2. *Nano Lett.* **2013**, *13* (8), 3626–3630. https://doi.org/10.1021/nl4014748.

(37) Zhou, Y.; Kiriya, D.; Haller, E. E.; Ager, J. W.; Javey, A.; Chrzan, D. C. Compliant Substrate Epitaxy: Au on MoS 2. *Phys. Rev. B* **2016**, *93* (5). https://doi.org/10.1103/PhysRevB.93.054106.

(38) Cheng, P.; Gu, W.; Shen, J.; Ghosh, A.; Beskok, A.; Hao, Z. Performance Study of a PDMS-Based Microfluidic Device for the Detection of Continuous Distributed Static and Dynamic Loads. *J. Micromechanics Microengineering* **2013**, *23* (8), 085007. https://doi.org/10.1088/0960-1317/23/8/085007.

(39) Kim, Y.; Cruz, S. S.; Lee, K.; Alawode, B. O.; Choi, C.; Song, Y.; Johnson, J. M.; Heidelberger, C.; Kong, W.; Choi, S.; et al. Remote Epitaxy through Graphene Enables Two-Dimensional Material-Based Layer Transfer. *Nature* **2017**, *544* (7650), 340–343. https://doi.org/10.1038/nature22053.

Acknowledgments

The authors thank Kevin Chen for helpful discussions, Matin Amani for assistance with electrical measurements, Naima Azgui for assistance with XPS measurements, and Penghong Ci for assistance with Raman measurements. Fabrication and electrical testing of devices was supported by the National Science Foundation, Award 1636256: SNM: Scalable Nanomanufacturing of 2D Electronic Materials and Devices Using Automated Exfoliation. Optical characterization was supported by the Electronic Materials Program, funded by the Director, Office of Science, Office of Basic Energy Sciences, Materials Sciences and Engineering Division of the U.S. Department of Energy, under contract no. DE-AC02-05CH11231. HMG acknowledges fellowship support from a National Science Foundation Graduate Research Fellowship under Grant No. DGE 1106400. SBD acknowledges the Lam Research Graduate Fellowship.

Author Contributions

HKT, JWA, DCC, and AJ developed the project. HMG, EMY, VDN, and HKT conceived of the method and devised processes for deploying the method. HMG carried out sample fabrication. JWA and CMT designed the optical characterization scheme and CMT performed optical characterization and data analysis. SBD fabricated transistors and HMG measured electrical characteristics. SBD assisted with interpretation of device data. ECL and HMG created monolayer boundary identification code. HS carried out molecular dynamics simulations. HMG, CMT, and HKT drafted the manuscript. All authors edited and refined the manuscript.

Supporting Information

Supplementary information is available in the online version of the paper: handle height calculations; MoS_2 photoluminescence characterization; Raman characterization; AFM topography, friction, and phase maps; XPS characterization; additional electrical characterization; comparison to existing exfoliation methods; and process yield details.

Competing financial interests

The authors declare no competing financial interests.

Table of Contents graphic:

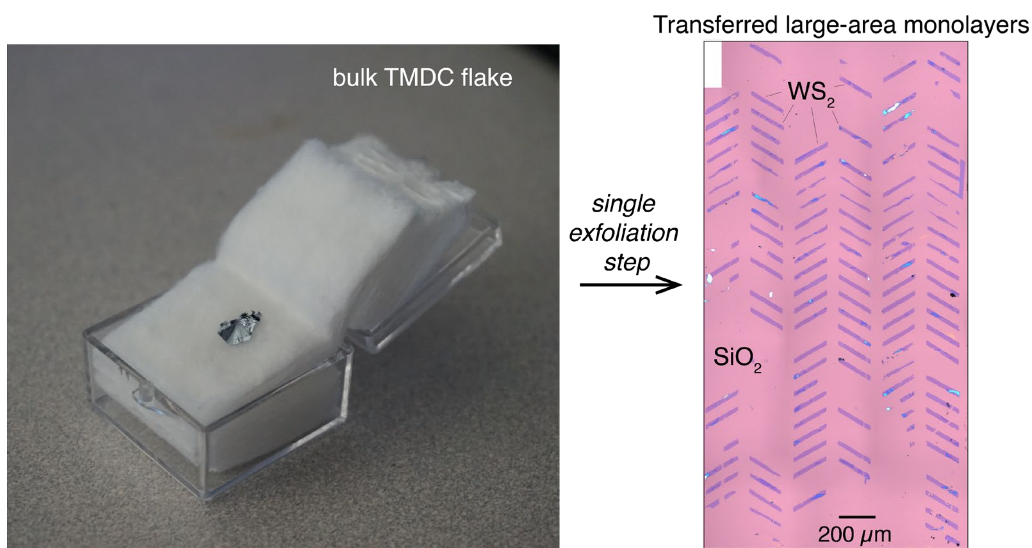

Supplementary Information

accompanying

Spatially precise transfer of patterned monolayer WS_2 and MoS_2 with features larger than 10^4 μm^2 directly from multilayer sources

Hannah M. Gramling,[1] Clarissa M. Towle,[2,3] Sujay B. Desai,[3,4] Haoye Sun,[2] Evan C. Lewis,[1] Vu D. Nguyen[1], Joel W. Ager III,[2,3] Daryl C. Chrzan,[2,3] Eric M. Yeatman,[5] Ali Javey,[3,4] and Hayden K. Taylor[1*]

[1] Department of Mechanical Engineering, University of California, Berkeley, Berkeley, CA 94720, USA

[2] Department of Materials Science and Engineering, University of California, Berkeley, Berkeley, CA 94720, USA

[3] Materials Sciences Division, Lawrence Berkeley National Laboratory, 1 Cyclotron Road, Berkeley, CA 94720, USA

[4] Department of Electrical Engineering and Computer Sciences, University of California, Berkeley, Berkeley, CA 94720, USA

[5] Department of Electrical and Electronic Engineering, Imperial College London, Exhibition Road, London SW7 2AZ, UK

* Correspondence and requests for materials should be addressed to H.K.T. (e-mail: hkt@berkeley.edu).

S1. Previously reported patterned two-dimensional material transfer processes

Reports in the literature of methods for transferring patterns of the most widely-studied van der Waals materials — graphene and MoS_2 — from multilayer sources, show considerable variability in transferred thickness, and inability to transfer a monolayer repeatably. Methods for depositing patterned MoS_2 from bulk sources are, as yet, unable to produce monolayers, while methods for depositing large-area MoS_2 result in randomly shaped pieces of material with low yield, and require post-processing (**Fig. S1**).

S2. Theory of metal film assisted exfoliation

A key feature of our process is the ability to reliably transfer monolayers using a single, controlled exfoliation step. This exfoliation process begins with the deposition of a thin metallic film (Au in this case) that mediates the process. Experimentally, it has been shown that the Au film can increase the monolayer selectivity of the exfoliation process, and also has the potential to exfoliate large-area samples.[26] We have developed a theory for the exfoliation process that explains the experimental observations and can be used to design films tailored to the exfoliation of specific materials.[30]

In brief, the metallic film does two important things to the exfoliated material. First, it strains only the top layer of the film that is to be exfoliated.[37] This strain leads to two important and sometimes competing effects. The strain changes the effective atomic density of the film. This alters the strength of the van der Waals force (on a per-area basis) between the top and subsurface layers of the exfoliated crystal. Tensile forces weaken the force, and compressive forces increase it. An increased force tends to pull the top layer closer to the second layer, and decreases monolayer selectivity for the exfoliation process. A decreased force has the opposite effect.

Second, the strain in the film also changes the stacking registry of the layer to be exfoliated. Because the lattice parameter of the strained to-be-exfoliated layer differs from that of the layer below, some regions of the exfoliated layer will be in unfavorable stacking positions relative to their initial positions. This weakens the bond between the exfoliated layer and layers beneath. The force density and stacking registry can sometimes compete against one another. In the case of the transition metal dichalcogenides studied here, the stacking registry changes dominate, and the strain, even though compressive, enhances monolayer selectivity of the exfoliation process.

The strain effects of the metallic film are present and play a role even in the exfoliation of nominally infinite monolayers. However, the monolayer-selective exfoliation and transfer of patterned films is further assisted by the additional stiffness of the metallic film. **Fig. S2** shows the exfoliation of a finite-width patterned strip modeled using LAMMPS[40]. The simulation uses a REBO potential developed for MoS_2 (slightly modified[30]) to examine the metal film-mediated exfoliation. In the simulations, a supercell composed of three layers of patterned MoS_2 strip and five layers of crystalline MoS_2 substrate has been constructed. The strip consists of 75×20 unit cells and the substrate consists of 100×19 unit cells. With these dimensions, each strip is approximately 24 nm in width and infinite in length (due to periodic boundary conditions). The separation between two strips is approximately 16 nm. The topmost layer of sulfur atoms have been biaxially strained 5%, and fixed in position in order to represent the forces arising from the deposited Au film. The bottom layer of sulfur atoms is also fixed, as noted in **Fig. S2.** The top layer is displaced in small increments, and the entire sample is equilibrated (at T = 0 K), and this process is repeated until the exfoliation event is observed. Interestingly, as the top layer is

moved, the point at which the to-be-exfoliated layer meets the second layer takes on a configuration resembling a crack. The monolayer then exfoliates through the propagation of this crack.

The exfoliation process, then, can be enhanced and controlled using the mechanisms identified in the paragraphs above. Based on this understanding, one should be able to design patterned exfoliation processes with enhanced monolayer selectivity for a broad range of 2D van der Waals-bonded materials.

S3. Required thickness of handle layer

During exfoliation of the photoresist/gold/TMDC stack from the multilayer source, there is a risk of the tape material deforming and penetrating the voids between handles. If any penetrating material were to come into contact with exposed vdW-bonded material during transfer, it could result in transfer of material occurring outside of the desired locations (**Fig. S3**).

We therefore model the adhesive deformation process to ensure that the handle is thick enough to prevent unwanted contact. The adhesive film consists of a solid backing layer of ~100 μm thickness coated with an adhesive layer that is ~50 μm thick. Here, because the adhesive layer is much less stiff than the backing layer, we conservatively model the adhesive as an elastic half-space having the properties of the adhesive layer. Modeling the adhesive as a half-space represents a conservative case because doing so will, if anything, overestimate deflections and hence the likelihood of unwanted contact being made. Nanoindentation measurements (TI 900 Hysitron TriboIndenter) give an adhesive layer mean Young's modulus of 3 MPa (measured at 30 μN load) and we assume a Poisson's ratio 0.5, translating to a plane strain modulus of 4 MPa.

The baked photoresist is an order of magnitude stiffer than the deformable component of the transfer medium ($E_{transfer\ medium}$ = 3–4 MPa; $E_{photoresist}$ = 36–40 MPa; both measured by nanoindentation), so we ignore photoresist deformation (<1% strain expected under uniaxial applied far-field stress σ_∞ = 300 kPa (details below), which corresponds to <150 nm of height compression) and consider only the deformation of the tape material into the regions between photoresist features.

The condition for roof collapse in a flexible 'stamp' with periodic rectangular protrusions is provided by C. Y. Hui, *et al.*[41], as solved using Muskhelishvili's method. For a stamp of protrusion (handle) width 2*a*, spacing 2*w*, and a material of plane strain modulus E^*, exposed to a given far-field stress σ_∞ (see **Fig. S3**), the required protrusion height (photoresist handle height) *h* to avoid roof collapse (*i.e.* unwanted contact) is given by

$$h > \left(\frac{-4\sigma_\infty}{E^*}\right)\left(\frac{2(a+w)}{2\pi}\right)\cosh^{-1}\left[\sec\left(\left(\frac{w}{2}\right)\frac{2\pi}{2(a+w)}\right)\right]. \tag{S1}$$

For features of width $2a$ = 40 μm and inter-feature spacing $2w$ = 100 μm, under an applied exfoliation pressure σ_∞ = 300 kPa (the minimum recommended pressure for ensuring good contact with a pressure-sensitive adhesive, in industry literature[42, 43]) a handle height of 9.9 μm is required. A spin recipe was developed to exceed the minimum acceptable value of *h* and provide 12–15 μm-thick handles. Thicknesses within this range were produced using a two-layer spin-coat process with AZ 4620 photoresist (see recipe in Section S8 below).

S4. Photoluminescence (PL) measurements

Substrates carrying transferred WS_2 or MoS_2 were characterized using photoluminescence spectroscopy in a custom micro-PL system (Lexel 95 argon ion laser, power: 0.35–0.37 μW; λ: 514.5 nm; NA: 0.8; spot size: 1.1 μm^2; filter: 550 nm long-pass). The power of the excitation beam was calibrated at high illumination intensity using a photodiode power meter (ThorLabs S120C). For the duration of the measurement, the excitation beam power was found to be 20 times the incident power on the sample. For PL spectra collection, the laser beam was focused onto the sample using a 50x objective lens (NA = 0.8) which resulted in a measured spot size of 1.1 μm^2 full-width half-maximum.

PL imaging data were collected through a 10x objective lens (NA = 0.3) using excitation from a GaInN LED (λ: 450 nm, power: 170 μW at sample) with the illumination distributed over a spot of diameter 1.8 mm, giving a power density of 65 $\mu W/mm^2$. Outgoing counts from the samples were collected through same microscope objective, passed through a 550 nm dielectric long-pass filter to remove the excitation signal, dispersed by an f = 340 mm spectrometer with a 150 g/mm grating, and detected by a Si CCD camera (Andor iDus BEX2-DD). Prior to measurements, the entrance slit of the spectrometer was opened until the maximum number of PL counts was obtained. The CCD background was obtained by collecting a spectrum before each measurement, over the same integration time as the eventual measurement, without the laser on. The background was subsequently subtracted from the PL spectra.

The measured PL spectra from the 13 measured locations on WS_2 have peak energies with a mean of 2.00 eV and a standard deviation of 0.021 eV. The PL spectra for WS_2 are shown in **Fig. 2(c)** of the main text. The peak energies are assumed to correspond to the optical bandgap of the material. The observed bandgap nonuniformity of barely 1% of the mean indicates that the material could be usable for constructing complex circuits with consistent performance across many devices. A two-tailed t-test assuming the measured bandgaps to be normally distributed finds that the optical bandgap of the transferred monolayer material is significantly lower ($p < 0.00025$) than the theoretically predicted value[44] of 2.03 eV for an unstrained, isolated monolayer. This slight red-shift is consistent with the effect of the proximity of a SiO_x substrate as reported previously[45], or with residual strain induced otherwise in the material[36].

For the MoS_2 samples, meanwhile, PL spectra are illustrated in **Fig. S4**, and the ten measured monolayer regions yield a mean peak energy of 1.875 eV with a standard deviation of 0.006 eV. As in the case of the transferred WS_2 monolayers, a two-tailed t-test finds that the optical bandgap of the transferred monolayer material is significantly lower ($p < 0.03$) than the theoretically predicted value[44] of 1.88 eV for an unstrained, isolated monolayer.

The results of PL imaging are shown in **Fig. 2(b)** and **Fig. S4(b)**. Those regions with any detectable PL signal correspond to regions identified from the associated white light reflectance images as containing monolayer material. Thus, although spatial uniformity of the imaged PL within monolayer regions is variable, the observation of PL is a reliable indicator that monolayer material is present.

Samples were treated in bis(trifluoromethane) sulfonimide (TFSI) superacid to determine whether this method could improve the quantum yield, as demonstrated previously for transition metal dichalcogenide monolayers[46]. The chip carrying the samples was treated in a 0.2 mg/mL solution of TFSI, in a mixture composed of dichloroethane and dichlorobenzene in a 10:9 ratio. The chip was submerged in this solution for 10 minutes at room temperature, then removed and dried with a jet of N_2. The superacid treatment increased the quantum yield by at least 25x in the case of WS_2, and at least 100x in the case of MoS_2, as evidenced by the large increases in PL

intensity in response to equivalent illumination intensities: results are shown in **Fig. 2(d)** for WS_2 and **Fig. S4(d)** for MoS_2.

S5. Raman measurements

Raman spectroscopy measurements were performed at 20× and 50× magnification in a Renishaw Raman system (λ: 488 nm, power: 1 mW at sample (50×), spot size: 1 µm diameter, grating: 2400/mm). In order to characterize large areas, Raman maps were constructed by collecting spectra at each point on a user-specified grid. The grid pitch varied based on magnification and the size of the area of interest. Raman maps and spectra on monolayer WS_2 and MoS_2 are shown in **Fig. S5** and **Fig. S6**, respectively.

The E_{2g} and A_{1g} peaks were identified using a custom MATLAB script, and the difference in Raman shift between peaks (in units of cm^{-1}) was used to verify material thickness[47]. The Raman results were compared to photoluminescence spectra and images to ensure that both measurements indicated monolayer material in the same locations. The expected inter-peak differences as a function of thickness and material are given below, using data from ref. 47.

(All entries in units of cm^{-1} unless noted otherwise)

	Monolayer (1L)			Bilayer (2L)			
	E_{2g}	A_{1g}	*Difference*	E_{2g}	A_{1g}	*Difference*	% change, 1L to 2L
WS_2	356	418	*62*	355	419	*64*	3%
MoS_2	385	403	*18*	383	405	*22*	22%

Though Raman peak shifts are most pronounced in the transition between one (1L) and two (2L) layers of a TMDC (as opposed to, say, between two and three layers), the total detectable change in inter-peak shift (combining the redshift of the E_{2g} peak and the blueshift of the A_{1g} peak) is only 3% in WS_2. There is no appreciable difference in intensity of the peaks between different thicknesses. Photoluminescence measurements, on the other hand, offer an orders-of-magnitude difference in intensity between 1L and 2L, with negligible differences in intensity from 2L to 3L and upwards. Thus, PL is a more robust and rapid means of differentiating 1L from 2L.

S6. Further electrical characterization

Back-gated MOSFET devices were fabricated using transferred material. The transferred monolayer material was used as the channel, evaporated nickel electrodes served as source and drain contacts, and the p-type silicon substrate and SiO_2 functioned as a back gate and a gate dielectric, respectively. Source and drain electrode geometries separated by 10 µm-long channels were defined via photolithography using AZ 4620 photoresist (MicroChem), followed by 40 nm of nickel evaporation and liftoff in acetone.

A total of 20 devices with functional monolayer MoS_2 channels were measured (Agilent 4155C Semiconductor Parameter Analyzer; Everbeing probe station and chamber) on two separate substrates, and their switching characteristics are shown in **Fig. S7.** The average characteristics of devices differ between the two chips: on Chip 1, the on/off current ratio is between 10^4 and 10^6 at the smaller V_{DS} of 50 mV, rising to between 10^5 and 10^7 at V_{DS} = 1 V. In Chip 2, however, the corresponding on/off current ratios are between 10^2 and 10^4 at V_{DS} =

50 mV, and between 10^3 and 10^5 at V_{DS} = 1 V. The fact that there is greater consistency between devices on a given substrate than between the devices on different substrates indicates the possibility of substantial property differences between mined molybdenite crystal specimens. Equally, the differences may result from substrate-to-substrate variability in the transfer process.

Switching characteristics of six WS_2 monolayer devices on a single substrate are shown in **Fig. S8**. At V_{DS} = 50 mV, the on/off current ratio is at most 10^2, while at V_{DS} = 1 V, the ratio is approximately 10^3 to 10^5.

S7. Yield

The yield of the process is characterized using two metrics: the *feature yield* and the *areal yield*. *Feature yield* refers to the number of features transferred with *any* material, as a proportion of the total number of features that could possibly have been transferred within a selected area. *Areal yield* measures, for features that were transferred, the amount of monolayer material in a given feature as a proportion of the total intended feature area.

The feature yield is calculated by assessing, by eye, from a white-light optical reflection micrograph whether *any* material is transferred in each intended feature, summing the number of features where material is transferred, and dividing the total by the number of features that could possibly have been transferred in the region defined by the intersection of the reflectance image's field of view with the boundary of the thermal release tape used. The boundary of the tape was always within that of the source material. Thus, the denominator of the feature yield calculation fairly captures the number of features that one could expect to observe in a 'perfect' transfer process. A single percentage yield is reported for a particular substrate.

The areal yield for a particular feature is calculated by determining, through image processing, the bounds of any monolayer regions in that feature, and dividing the total area of any such region(s) by the area of the corresponding intended feature on the photomask used for initial patterning. By considering the set of these ratios for all transferred features on a given sample, a mean areal yield as well as a standard deviation are reported. Monolayer regions are determined by (1) identifying, by eye and based on experience, the characteristic color and contrast (relative to the substrate) of monolayer material in the image; (2) using an image segmentation function in Matlab together with custom-written code to calculate the areas of all regions with close to that characteristic color and contrast. Results were manually verified by comparison with PL images, and it was confirmed that identified monolayer regions corresponded to those regions with any appreciable intensity in the PL images. The code is sensitive to step changes in color intensities, and bilayer and thicker regions were consistently identified as non-monolayer. Extracted monolayer areas were also used to generate the histograms in Fig 3 of the main text.

The feature and areal yields for three WS_2 and eight MoS_2 samples are shown in **Table S1**. Feature yield ranges up to 67% for WS_2 and up to 54% for MoS_2. Mean areal yields of 63% for WS_2 and 55% for MoS_2 are obtained. Yield from the WS_2 is markedly higher than that from the MoS_2, which we attribute to the greater uniformity and flatness of the initial, synthetic, WS_2 source than the natural MoS_2 crystal.

S8. Photolithography

AZ 4620 photoresist was spun onto the gold-evaporated surface of bulk MoS_2 and WS_2 flakes using a two-layer process:

	RAMP 1	SPEED 1	TIME 1	RAMP 2	SPEED 2	TIME 2
SPIN 1	100 rpm/s	500 rpm	10 s	500 rpm/s	2400 rpm	60 s
SPIN 2	100 rpm/s	500 rpm	10 s	500 rpm/s	1600 rpm	60 s

The resist was baked at 110 ºC for three minutes following each spin. The resist was exposed with a chrome/glass contact transparency mask for 10 seconds at approximately 20 mW/cm^2 and subsequently developed for four minutes in AZ 400K developer pre-diluted 1:3 with deionized water.

S9. Atomic force microscopy

Atomic force microscopy measurements (Bruker ScanAsyst, tapping mode) confirm that the transferred material regions identified as monolayer material by optical microscopy and photoluminescence spectroscopy are in fact sub-1-nm thick (**Figs. S9 and S10**). Narrow, steep regions are present at the edge of each feature. These may be curled monolayer material, which are observed throughout the feature if the substrate surface is insufficiently hydrophilic during exposure to liquid (KI/I_2 and DI water), driving liquid under the transferred monolayer. Phase and tapping-mode (TM) friction measurements were collected from the same topography-mapped regions, on both WS_2 and MoS_2 monolayers.

The particles arrayed on both the transferred material and the substrate are approximately 5 nm tall; XPS analysis indicates that they are gold remnants remaining after the final gold removal step (see Section S10). In order to determine whether these particles impact the ability to fabricate atomically coupled heterostructures, Raman spectroscopy was performed on "bilayers" created by stacking two successive monolayer transfers with the process described in this work (see Section S3). Initially, a Raman spectrum of the stacked material indicates that the stack behaves as two monolayers (**Fig. S12**); however, after brief exposure to heat (3 minutes at 150 ºC, followed by 3 minutes at 200 ºC), a Raman spectrum collected from the stacked material shows an inter-peak distance characteristic of an MoS_2 bilayer (see Section S6). Though preliminary, these measurements indicate that the monolayers can functionally couple despite the gold remnants. From an electronic perspective, the demonstrated switching ability of transistors formed using transferred monolayers (see Section S7) confirms that the remnants do not short devices. At shorter channel lengths, however, the remnants may pose a challenge. Extended KI/I_2 acid treatment of the surface, possibly coupled with one or more of mechanical agitation, sonication, and an extended or more vigorous water rinsing protocol afterwards could assist in residue removal.

S10. X-ray photoelectron spectroscopy (XPS) characterization

XPS (Perkin Elmer PHI 5600 ESCA System with neutralizer, spot size: 800 µm diameter, source power: 400 W) was used to identify the materials present on the surface of fabricated arrays of transferred monolayers, and in particular to identify candidate elements for the nanoscale particles detect using AFM. XPS was chosen for its sensitivity to surface material.

Tungsten and sulfur (TMDC monolayer), silicon and oxygen (substrate material), and carbon (adventitious carbon[48]) were expected in the measurement. The most pronounced unexpected peak corresponds to the 4p3 orbital of gold. Though the gold used in the process is

removed during a final KI/I_2 etchant exposure (see Section S1, step 10), it is possible that nanoscale particles remain on both the transferred monolayer and the silicon oxide substrate surfaces.

References

40. LAMMPS Molecular Dynamics Simulator: lammps.sandia.gov.

41. Hui, C. Y. *et al.*, Constraints on Microcontact Printing Imposed by Stamp Deformation. *Langmuir* **18,** 1394–1407 (2002).

42. 3M Corporation, Five Common Reasons Manufacturers are bonding with Industrial Tapes. *Advanced Manufacturing* (2017). Available online at: https://advancedmanufacturing.org/sponsored-3m-five-common-reasons-manufacturers-bonding-industrial-tapes/. [Accessed Jul. 29, 2018].

43. 3M Corporation, 3M™ EMI Shielding and Grounding Foil Tape AL39UL. (2012). Available online at: https://multimedia.3m.com/mws/media/875500O/3mtm-emi-shielding-and-grounding-foil-tapeal39ul.pdf?&fn=05723.pdf. [Accessed Jul. 29, 2018].

44. Gusakova, J. *et al.*, Electronic Properties of Bulk and Monolayer TMDs: Theoretical Study Within DFT Framework (GVJ-2e Method). *Phys. Status Solidi A* **214**, 1700218 (2017).

45. Liu, B. *et al.*, Engineering Bandgaps of Monolayer MoS_2 and WS_2 on Fluoropolymer Substrates by Electostatically Tuned Many-Body Effects. *Advanced Materials* **28** 6457–6464 (2016).

46. Amani, M. *et al.*, Near-unity photoluminescence quantum yield in MoS_2. *Science* **350** (6264), 1065-1068 (2015).

47. Saito, R. *et al.*, Raman spectroscopy of transition metal dichalcogenides. *J. Phys. Cond. Mat.* **28** (35), 353002 (2016).

48. Barr, T. and S. Seal, Nature of the use of adventitious carbon as a binding energy standard. *JVST A* **13**, 1239 (1998).

49. Liang, X. *et al.*, Plasma-assisted printing and doping processes for manufacturing few-layer MoS_2-based electronic and optoelectronic devices *in 25th Annual SEMI Advanced Semiconductor Manufacturing Conference* (IEEE ASMC, 2014).

50. Li, D. *et al.*, Nanoimprint-assisted shear exfoliation plus transfer printing for producing transition metal dichalcogenide heterostructures. *JVST B* **34** (6), 06KA01 (2016).

Figures

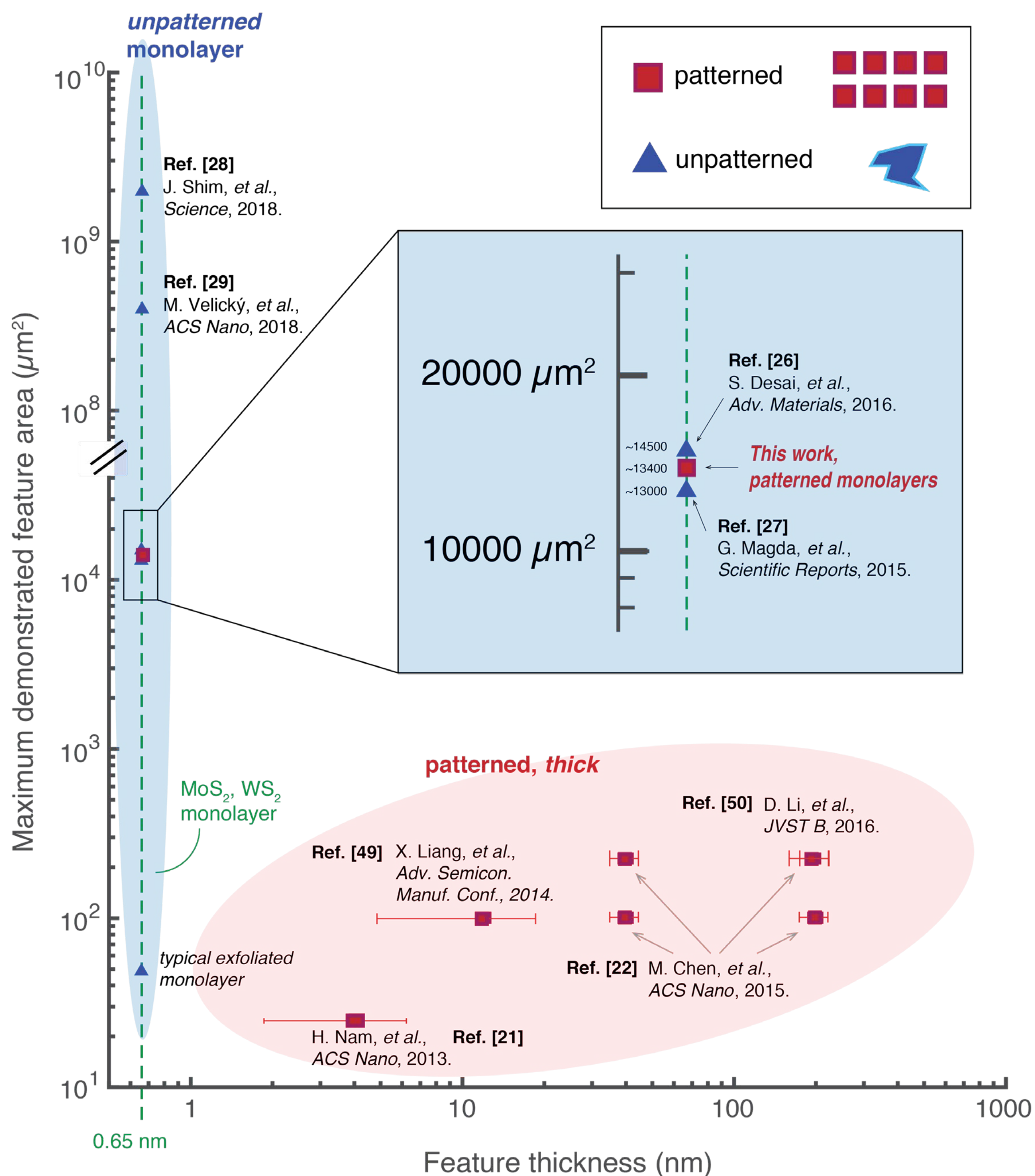

Figure S1. Our work demonstrates, for the first time, the combination of excellent monolayer selectivity with large (>10^4 μm) continuous areas of *shape-controlled* transferred material. Methods that produce flakes of uncontrolled size and shape are shown with blue triangles. These methods are capable of producing monolayers. Techniques that generate patterned arrays of MoS_2 features prior to deposition on the substrate are shown as red squares, with error bars indicating reported variation in layer thickness. Previously, two regimes were achievable: large, single monolayers of uncontrolled shape (blue oval) and arrays of thick material in controlled shapes and locations (red oval). Until now, no such patterned methods have been capable of generating repeatable monolayer thickness. The present work is included for comparison, demonstrating the generation of patterned monolayers.

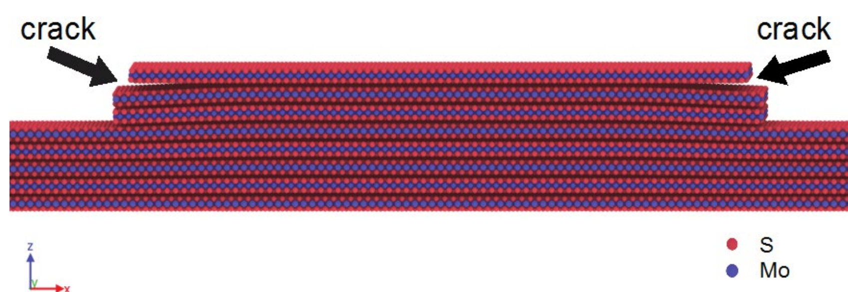

Figure S2. Molecular dynamics simulations elucidate the gold-mediated exfoliation mechanism. The exfoliation of a finite width strip bonded by gold film is viewed at the atomic scale. The bottom sulfur atoms are fixed, and the top sulfur atoms are strained and held in place to mimic the effect of a gold film. The top layer is then displaced in direction normal to the film. Note that a crack has opened at the edge of the strip. The sample exfoliates by propagation of this crack.

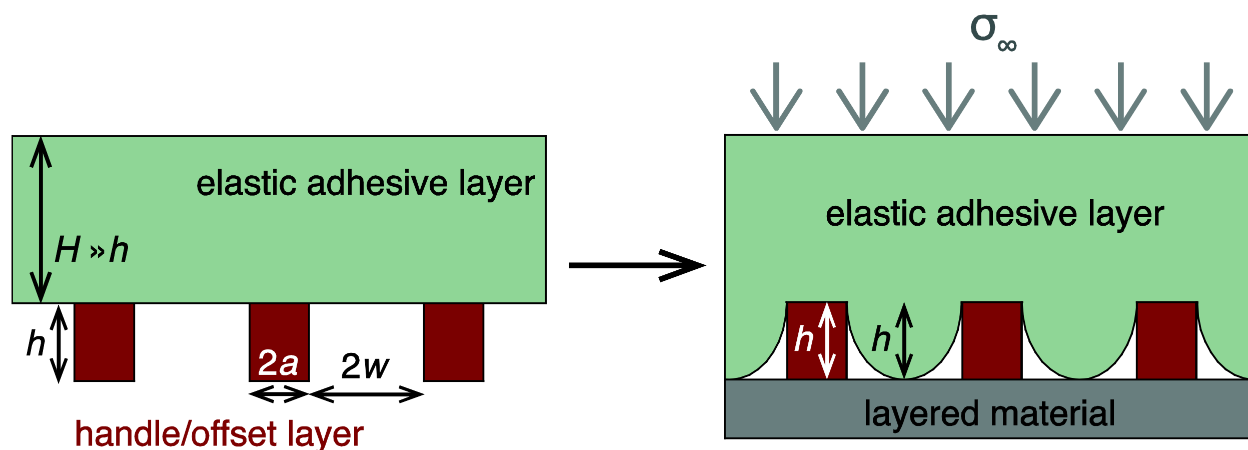

Figure S3. Dimensions of the photoresist handle layer are designed to prevent unwanted adhesive contact outside the handles. Dimensions of the handle layer (photoresist) pattern, in red, and the transfer medium (thermal release tape), in green, are shown. For a given far-field applied stress σ_∞, and adhesive layer material properties, a certain minimum h is needed to prevent unwanted, direct contact between the transfer medium and the unmasked vdW-bonded, layered material.

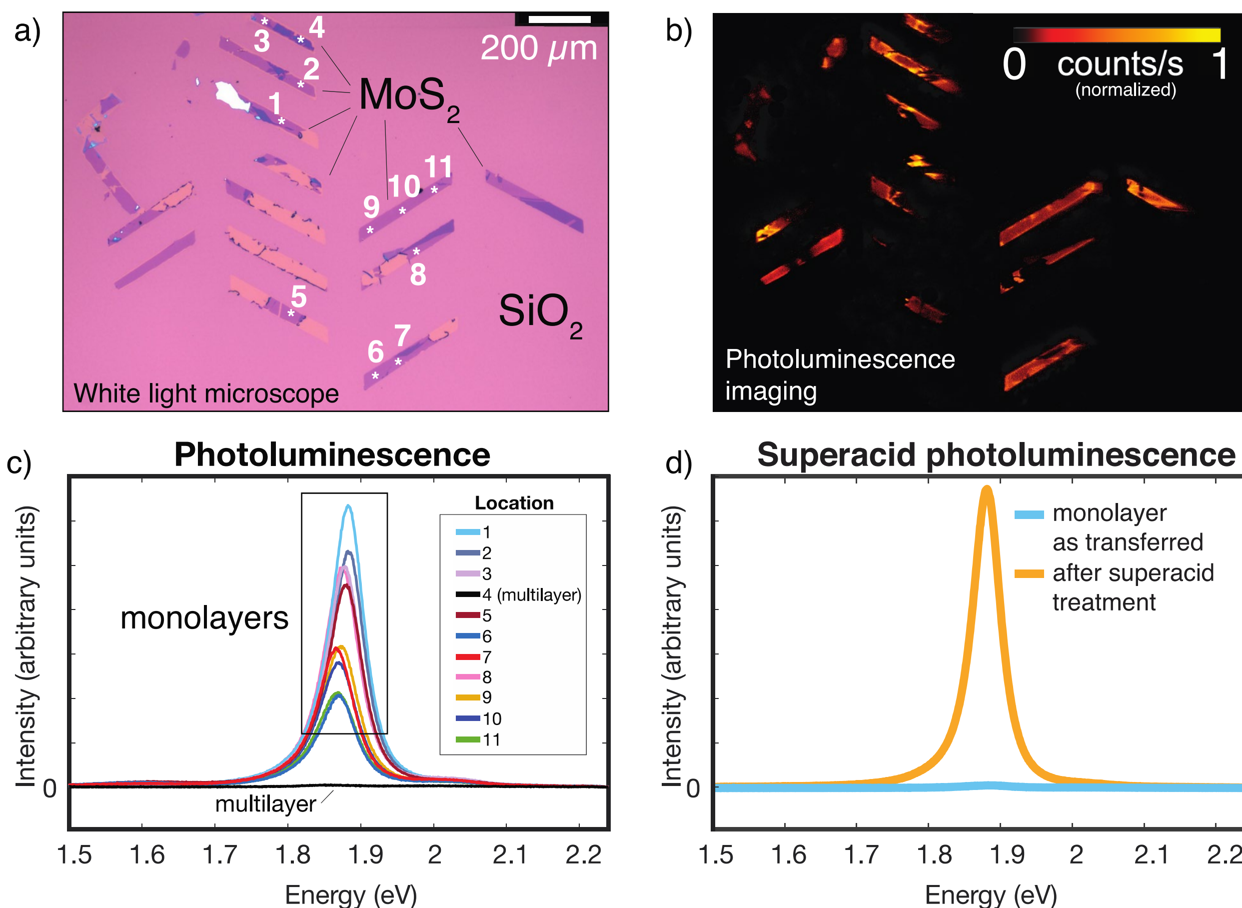

Figure S4. Optoelectronic MoS_2 monolayer characterization. (a) White-light reflectance image of a set of transferred MoS_2 features on 260 nm thermal SiO_2 on Si; (b) photoluminescence image of the region; (c) photoluminescence spectra associated with the numbered locations in (a), confirming that monolayer MoS_2 has been transferred to the substrate; (d) the results of treating MoS_2 monolayers with a superacid, showing more than a one hundred-fold increase in quantum efficiency.

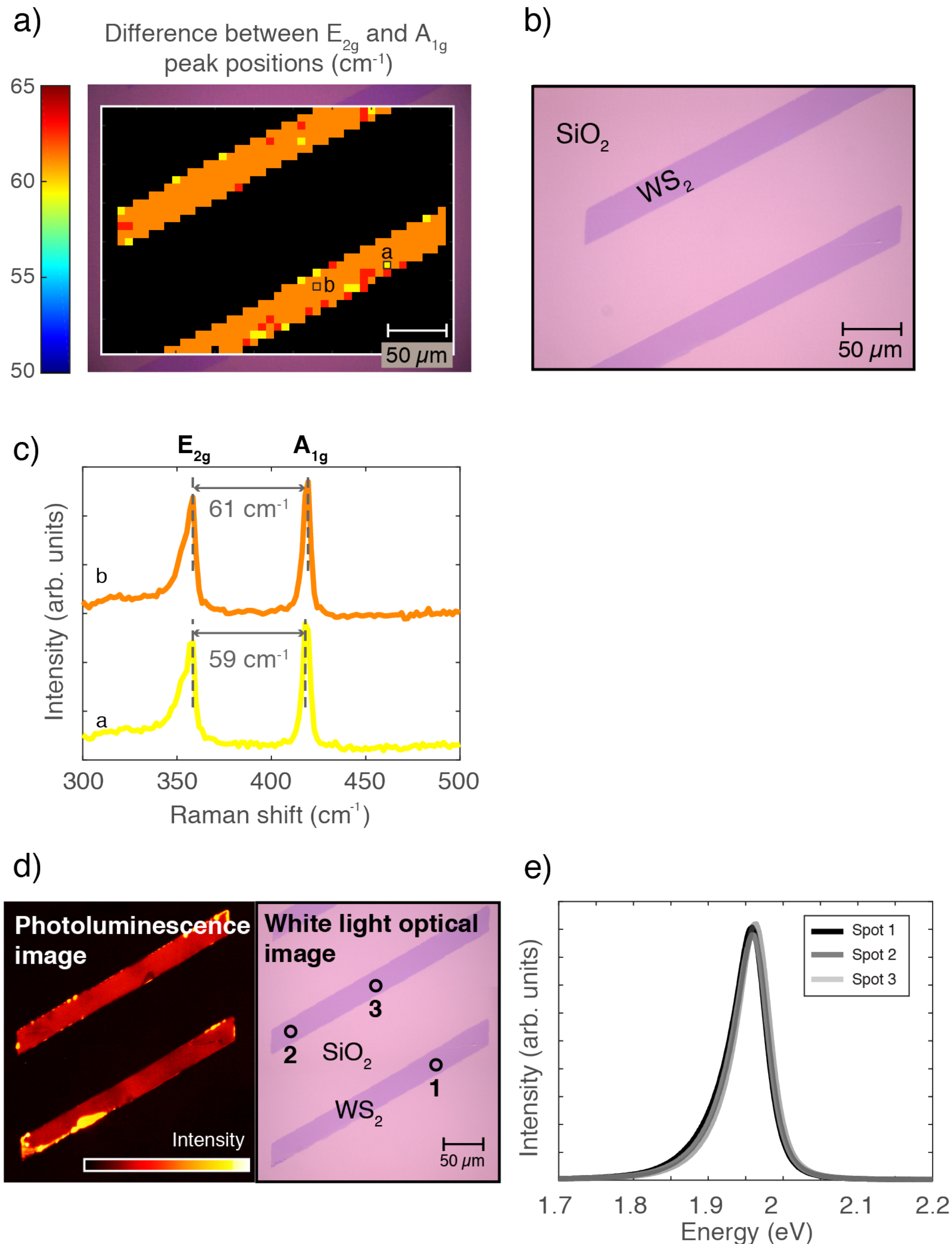

Figure S5. (a) Raman map of the E_{2g} and A_{1g} peak separation, indicative of material thickness, over two monolayer chevrons of transferred WS_2. (b) Optical image of the region measured in (a). (c) Spectra from two different regions, a and b, labeled in the map, showing inter-peak differences below the expected bilayer peak difference of 64 cm^{-1}. (d) Photoluminescence image (left) and optical image (right) of the same features mapped with Raman spectroscopy in (a). The readily observed luminescence across both features indicates their monolayer composition. (e) Unnormalized photoluminescence spectra from the three points labeled in (d), showing the consistent luminescence across the features.

MoS_2

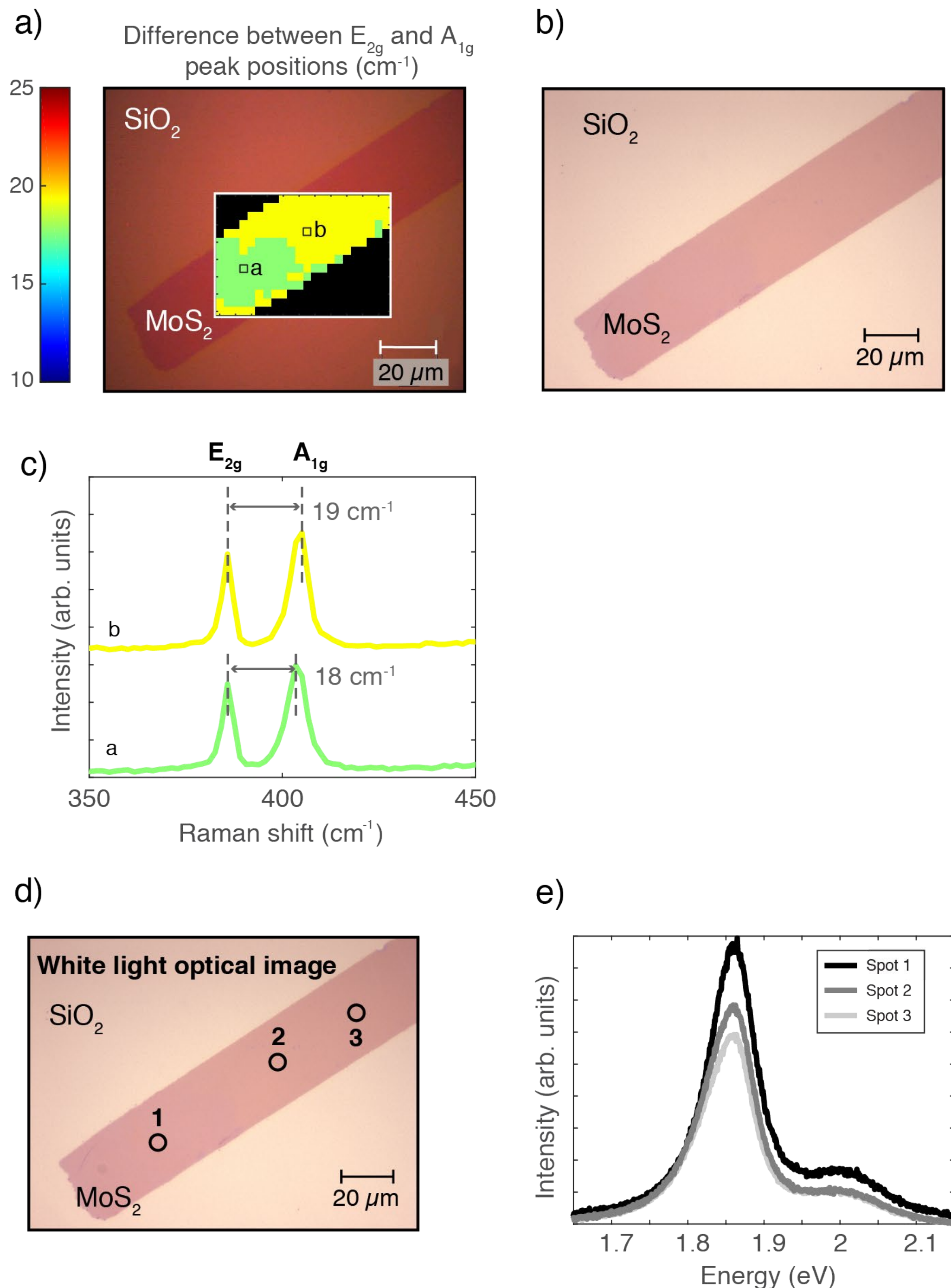

Figure S6. (a) Raman map of the E_{2g} and A_{1g} peak separation, indicative of material thickness, over a monolayer chevron of transferred MoS_2. The extent of the map scale is the same as in Figure S5. (b) Optical image of the region measured in (a). (c) Spectra from two different regions, a and b, labeled in the map, showing two inter-peak differences below the expected bilayer peak difference of 22 cm^{-1}. (d) Optical image of the feature mapped with Raman spectroscopy in (a), with points whose photoluminescence spectra were measured (e) labeled. (e) Unnormalized photoluminescence spectra from the three points labeled in (d).

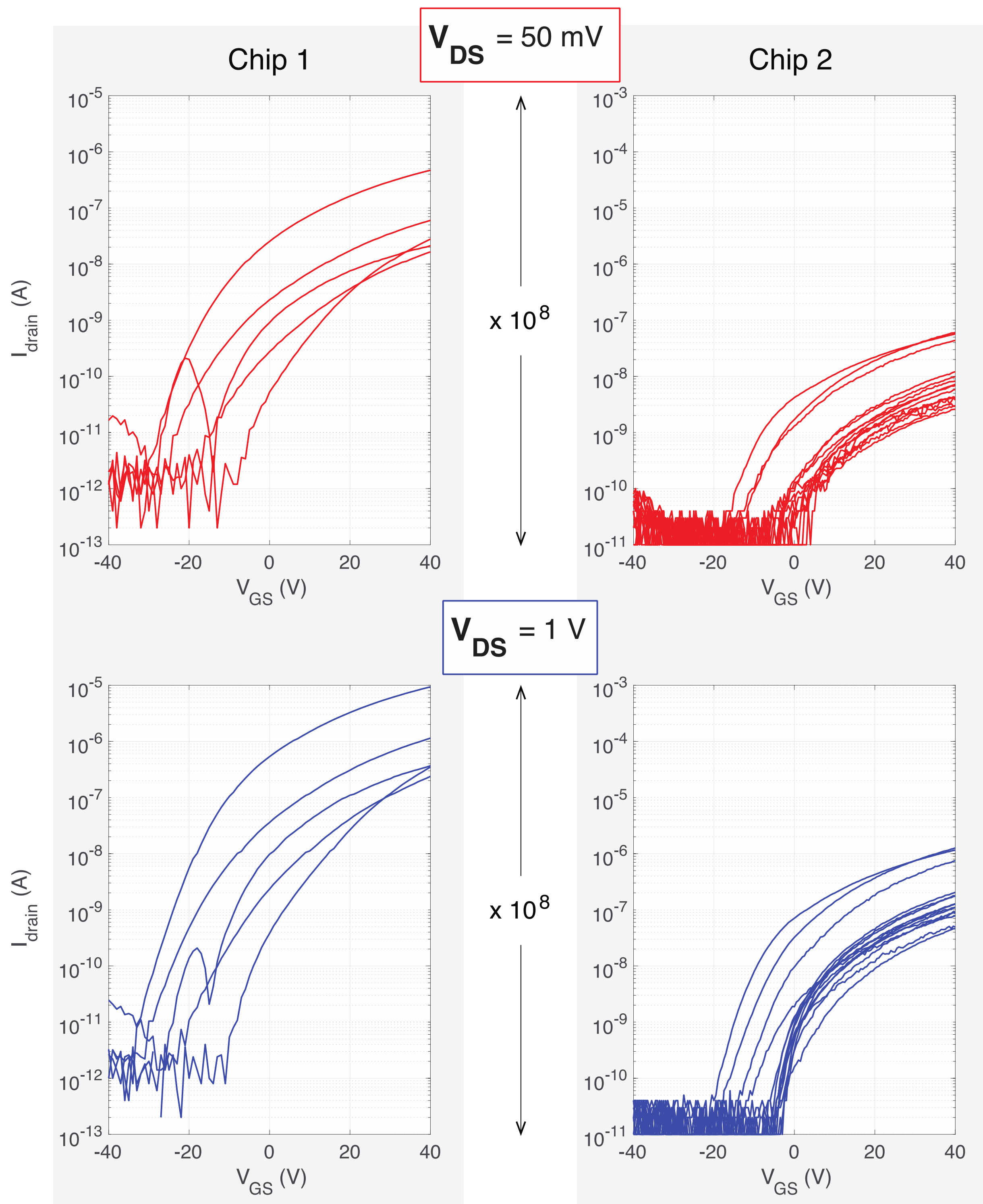

Figure S7. Switching characteristics of back-gated MoS_2 devices fabricated on two separate chips, using transferred monolayer MoS_2 channels from two separate initial mined MoS_2 sources. Chip 1 and Chip 2 are from different sources of material; five devices were measured on Chip 1 and 15 devices on Chip 2.

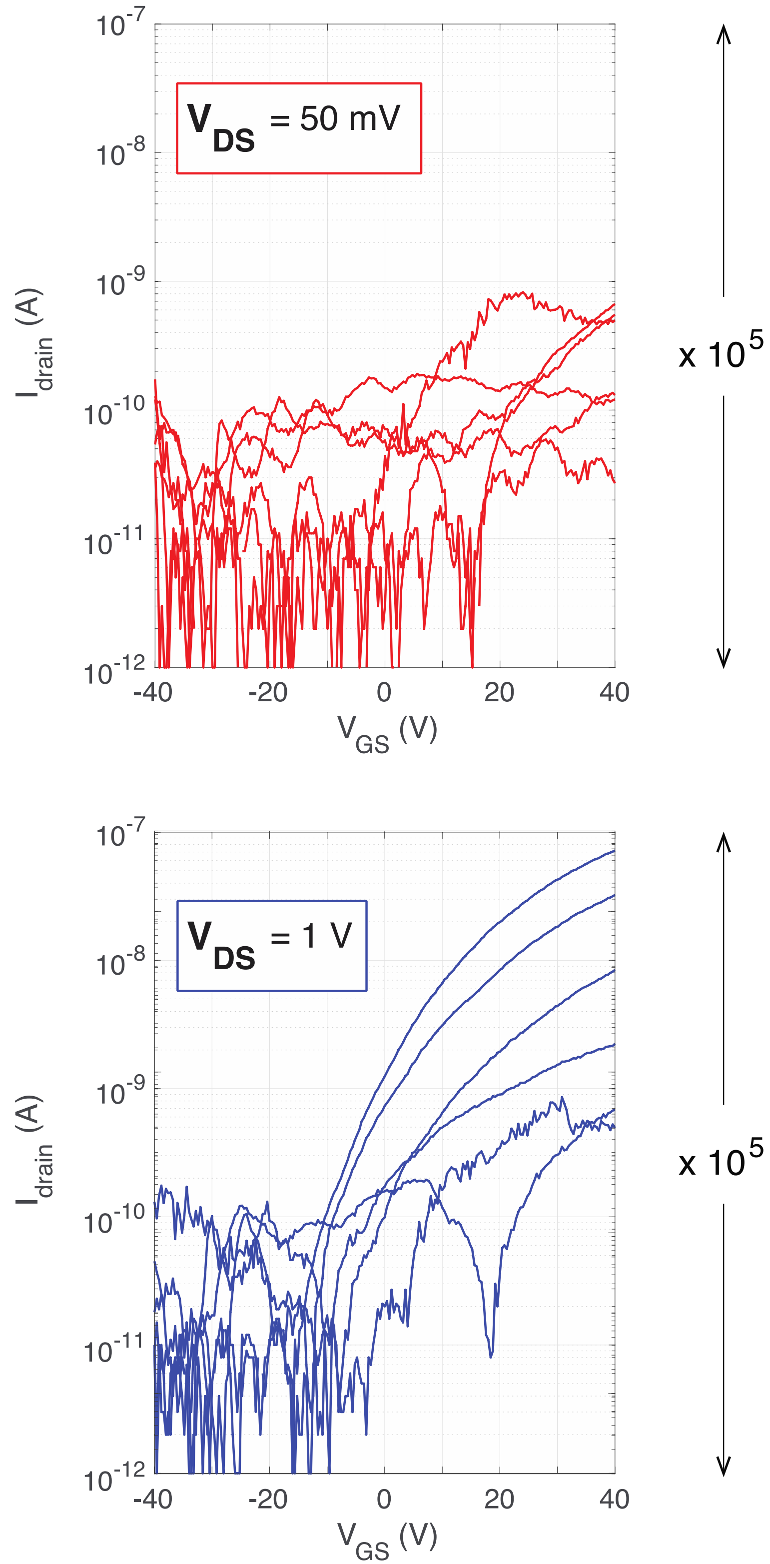

Figure S8. Switching characteristics of six back-gated WS_2 devices fabricated from monolayer WS_2 transferred from a synthetic bulk source.

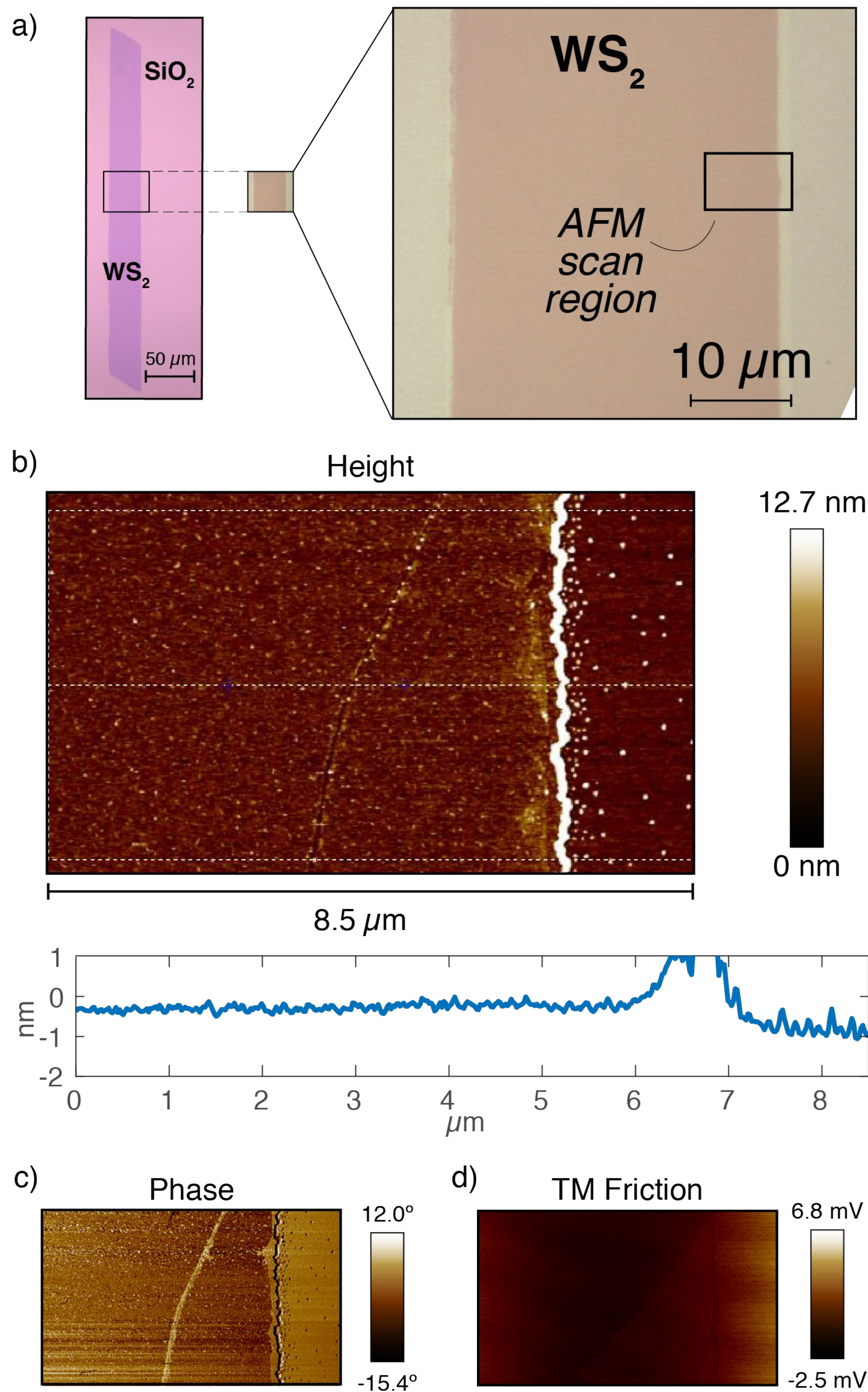

Figure S9. (a) White light optical image of the WS_2 monolayer region measured with atomic force microscopy. (b) topographical map measured by atomic force microscopy in tapping mode, with an averaged trace shown below indicating a ~6 Å step height between the substrate and the transferred monolayer. (c) AFM phase lag map and (d) friction map of the same region.

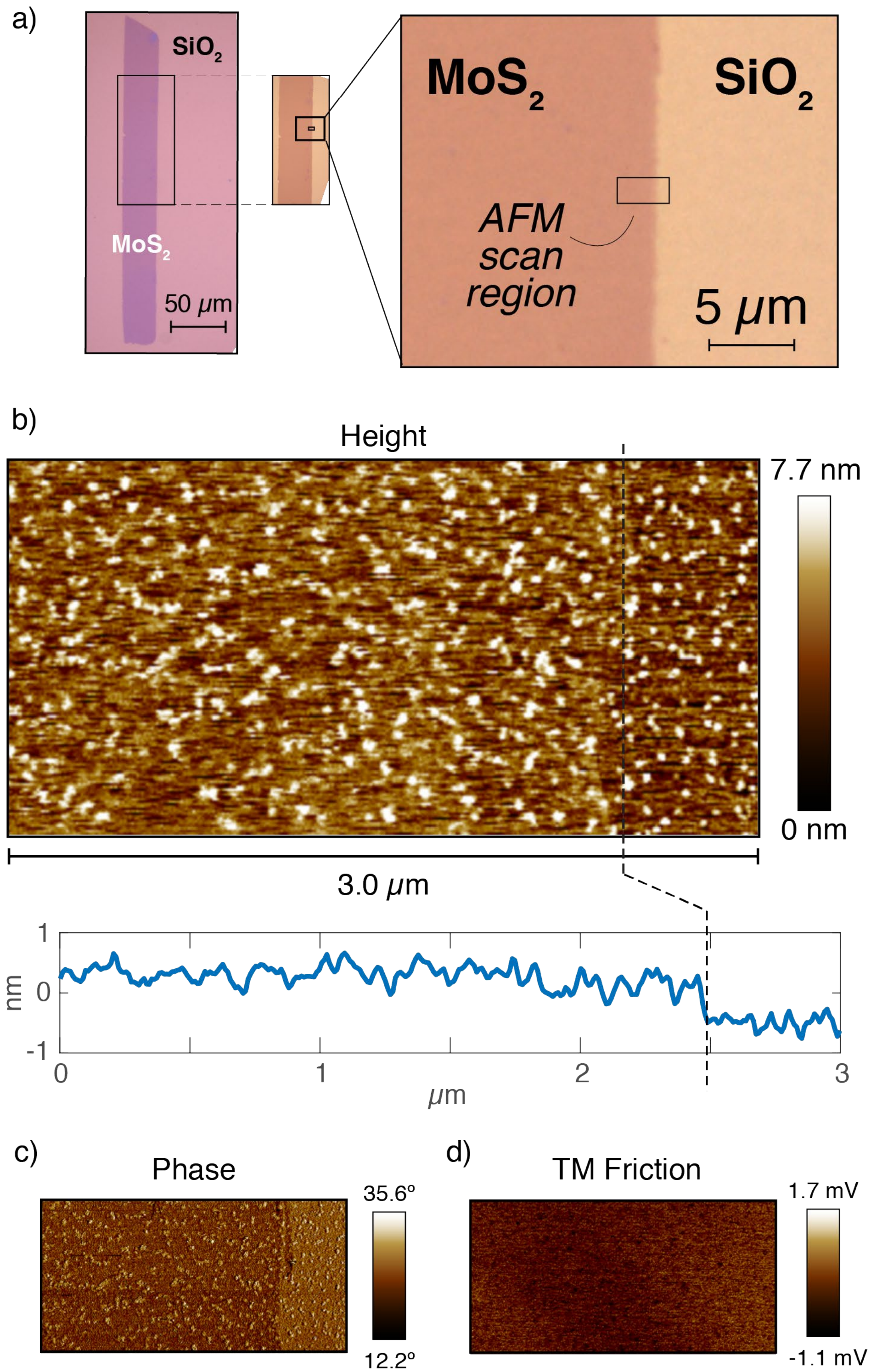

Figure S10. (a) White light optical image of the MoS_2 monolayer region measured with atomic force microscopy. (b) topographical map measured by atomic force microscopy in tapping mode, with an averaged trace shown below indicating a ~6 Å step height between the substrate and the transferred monolayer. (c) AFM phase lag map and (d) friction map of the same region.

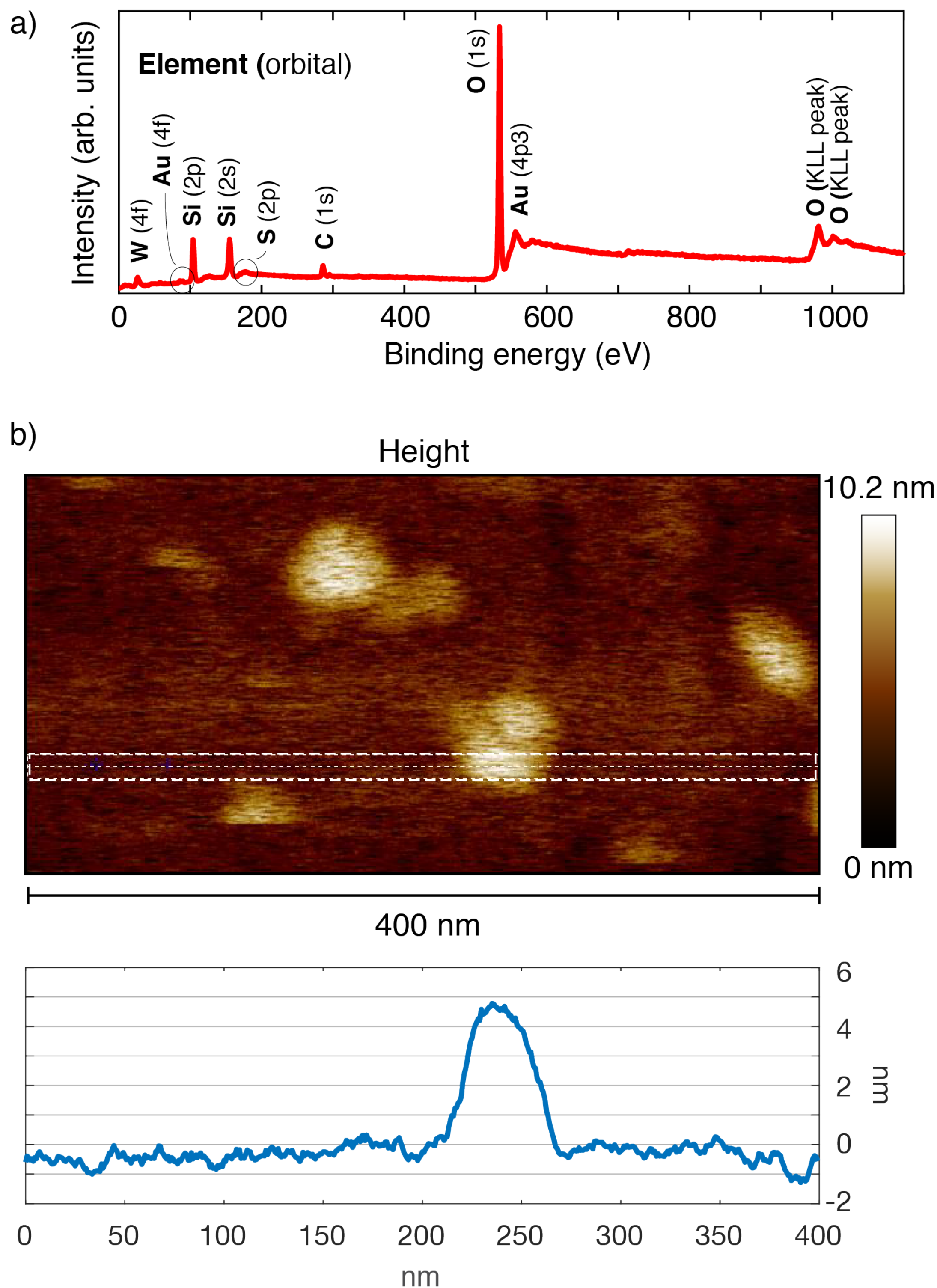

Figure S11. (a) XPS characterization of residual particles on WS_2, indicating the presence of expected substrate elements (Si, O), TMDC elements (W, S), and calibration elements (C). The remaining identified element is Au, which may comprise the residual particles. (b) AFM topography map of the particles. The height of the region in the white dashed box is plotted in the accompanying line-scan, showing that the particles are ~50 nm wide and ~5 nm tall.

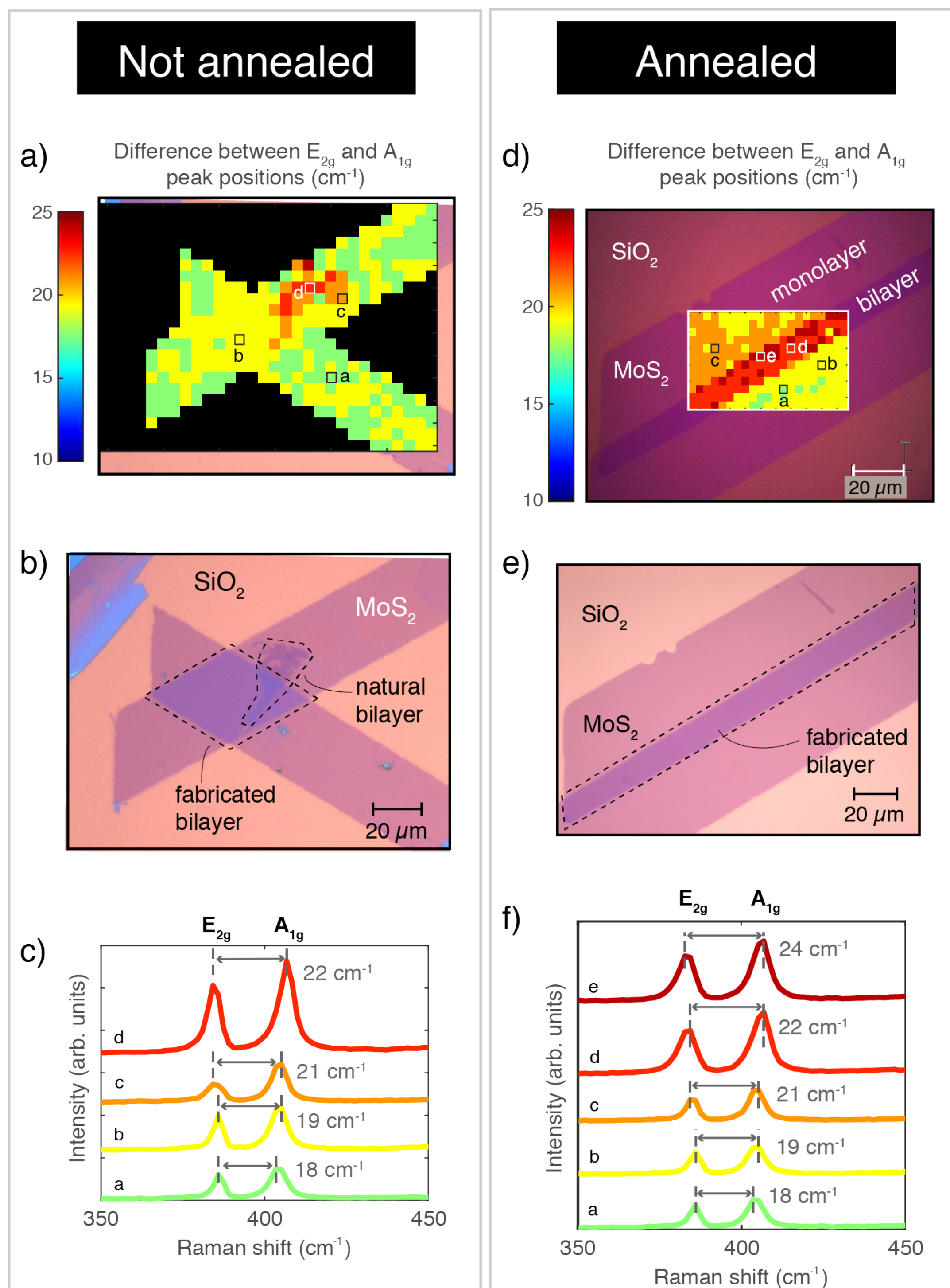

Figure S12. (a) Raman map of two crossed MoS_2 monolayer features, whose overlap forms a fabricated MoS_2 bilayer. The inter-peak difference is consistent with monolayer MoS_2, except in the region where a natural bilayer is present, highlighted in (b). (c) Spectra from several points on the Raman map, indicating both monolayer and bilayer material are present. (d) Raman map of two overlapped MoS_2 monolayers, creating a fabricated bilayer, after a brief annealing step. The overlapping region now behaves as an MoS_2 bilayer, as indicated by the increased E_{2g}-A_{1g} peak difference (in cm^{-1}). (e) The region mapped in (d). (f) Spectra from identified points of the region mapped in (d).

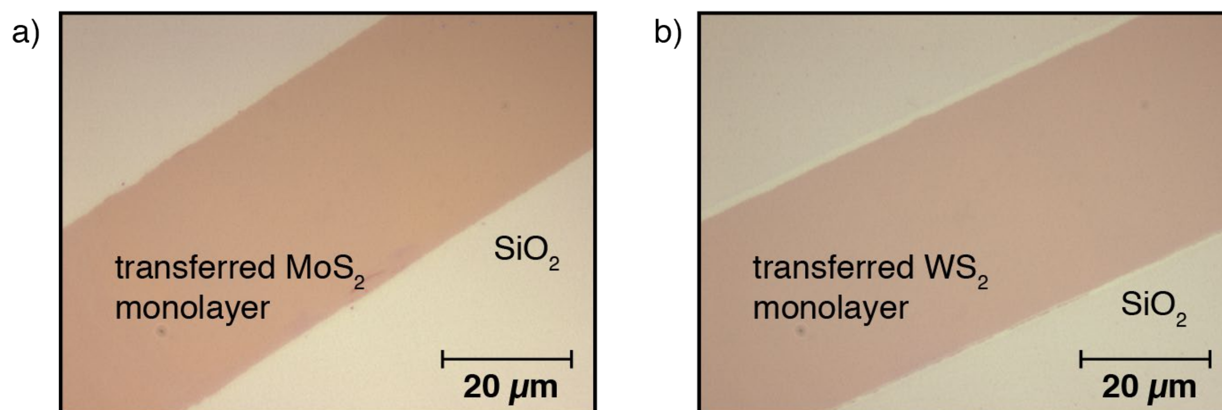

Figure S13. High-magnification white light optical images of a) MoS_2 and b) WS_2 monolayers on 260 nm SiO_2 substrates, produced using the transfer method described in this paper.

Table S1. Feature and areal yield calculations for eight representative MoS_2 and three WS_2 substrates, processed using the technique detailed in Fig. 1 of the main text. These substrates include those described by the histograms in Fig. 3 of the main text; where applicable, the corresponding histogram label in Fig. 3 is given in the rightmost column of this table.

	Sample	**Feature yield** (% features transferred)	**Areal yield** (% monolayer)		**Corresponding histogram in Fig. 3 of main text**
			Mean	Sample standard deviation, *s*	
WS_2	**1**	29/119 = **24%**	**63%**	**27%**	**A**
	2	52/95 = **55%**	**28%**	**18%**	**B**
	3	121/180 = **67%**	**53%**	**29%**	**C**
MoS_2	**1**	12/24 = **50%**	**35%**	**19%**	
	2	22/66 = **33%**	**40%**	**26%**	
	3	13/42 = **31%**	**25%**	**19%**	
	4	7/65 = **11%**	**55%**	**30%**	
	5	13/32 = **41%**	**47%**	**23%**	
	6	14/26 = **54%**	**31%**	**19%**	**D**
	7	29/75 = **39%**	**22%**	**17%**	**E**
	8	30/136 = **22%**	**40%**	**27%**	**F**

Berkeley, CA
December 10, 2018

Responses to reviewer comments on *Spatially precise transfer of patterned monolayer WS_2 and MoS_2 with features larger than 10^4 μm^2 directly from multilayer sources*

We are grateful to the reviewers for the constructive comments that they provided. Below we give our responses and describe the modifications that we have made to the manuscript, where necessary, to address them. Modifications to the text are shown in blue in the marked-up version of the manuscript.

Reviewer comment	*Response*
Reviewer 1	
1. The reason for debonding of 2D materials of the target substrate should be identified. At which step does the debonding happen and why? During the first exfoliation? Or during the rest of the process (etching and other processes)? How can this be improved?	We have actually observed that three different steps during the process contribute to yield loss, via either a debonding of the 2D material from the target substrate, or a failure to bond in the first place. We have added to the manuscript a new subsection ("Sources of yield loss" beginning on p.15) describing the three yield-limiting steps that we have identified, and offer suggestions for possible process modifications to address them. The added text is reproduced below: "We have identified three processing steps that contribute most significantly to yield loss, and that would therefore be a reasonable focus of future process development. Firstly, in step 5, some of the patterned photoresist handles do not adhere to the thermal release tape and therefore remain on the source crystal. This source of defectivity is evident from optical examination of the thermal release tape between steps 5 and 6, in which gaps are visible in the array of features on the tape. Strengthening binding between the PR handles and the adhesive film would help to address this issue, *e.g.* by applying a partially baked PR layer to the tape. Secondly, in some features, the photoresist–gold bond fails during step 5 and the gold and 2D layer therefore remain on the source crystal even when the photoresist feature is transferred to the tape. This source of defectivity is again evident from optical examination of the thermal release tape immediately after step 5, in which some of the photoresist features are visible but without the highly reflective gold layer on them. To address this source of yield loss, adhesion of the photoresist to the gold should be enhanced, potentially by adding an O_2 plasma or hexamethyldisilazane (HMDS) treatment between steps 1 and 2, although this has not yet been tried. Thirdly, in some locations where gold polygons are visible on the substrate after step 9, optical reflectance imaging after step 10 shows that the MoS_2 or WS_2 is ultimately absent from those same locations. We attribute this component of yield loss to ingress of KI/I_2 liquid between the 2D layer and the substrate during the gold etch of step 10, washing the 2D material off the substrate. This explanation is more plausible than earlier failure of the gold–2D material interface, since that interface is formed during the gold evaporation and is known

	to be strong because of the Au–S bond. We found that limiting the time that elapses between step 9 (exposing the substrate and its contents to O_2 plasma) and step 10 (gold KI/I_2 processing) to below an hour greatly mitigates this third yield limitation, resulting in the yield values reported above. Nevertheless, further refining this apparently critical plasma treatment step and/or thermally annealing the substrate before the final gold etch may be beneficial in improving the yield of step 10 beyond the values presently reported." We have also added text at the start of the Methods section (subsection: "Overview and novelty") in an effort to communicate more clearly the nature of the single exfoliation step that is involved in the process.
2. The author should explain the implications of the residue generated in the process. Au or any other contamination. How do it affect the potential applications and how to improve the current situation?	We have amended the Results and Discussion as follows to address this matter. In brief, we have seen no evidence of any adverse effects of these residues: "Our FET device characterization measurements have confirmed that our test devices, which have 10 µm channel lengths, exhibit strong switching behavior. The residues are therefore evidently sparse enough not to inhibit operation of devices at the 10 µm length-scale. Our XPS analysis of the residue (Section S9) indicates that it is gold; it is therefore conceivable that as devices are scaled down, the residue might provide a current-shorting path, but such behavior has not been observed. Another potential concern might be that surface residues could inhibit the formation of planar heterostructures requiring atomically-spaced layers. To examine this possibility we formed a planar interface between two MoS_2 monolayers that were transferred sequentially using our process followed by thermal annealing (details in supporting information, Section S9). The Raman spectra measured at multiple locations on this constructed bilayer are consistent with bilayer material—and *not* with two separate monolayers—which indicates that the layers became atomically close after transfer and annealing. Such behavior indicates that whatever residues were on top of the first-deposited MoS_2 layer did not inhibit the formation of intimate contact between it and the second-deposited MoS_2 layer. It is probable that the residues are so sparse that a monolayer of a 2D material can easily conform to them. The XPS evidence that these residues are gold suggests that they could be removed, if necessary, by modification of the final gold etching step, *i.e.* step 10 of the process. Extended KI/I_2 acid treatment of the surface, possibly coupled with one or more of mechanical agitation, sonication, and an extended or more vigorous water or solvent rinsing protocol could assist in residue removal. Certainly for the use of this process in combination with traditional silicon electronics, any gold residue would need to be very thoroughly removed, but for

	novel circuit integration based entirely on 2D materials, it is not yet known how much of an issue Au contamination may be.”
Reviewer 2	
In this work, the authors present a transfer printing approach that is capable of exfoliating large prepatterned monolayer WS2 and MoS2 structures (1e4 um^2) from bulk sources and subsequently printing them onto other substrates. This approach is very important for making TMDC-based functional devices on the special substrates that cannot be directly subjected to CVD growth processes (for example, flexible plastic substrates for wearable electroncs). This technique, if further optimized with a higher yield and reliability, could provide a transformative impact to the device fabrication based on emerging layered TMDC materials. Although this presented technique has a high novelty and could interest a broad range of audience, the current manuscript is too sketchy and lacks some necessary details for convincing TMDC device society with important scientific insights.	To make the presentation of the technique more concrete, we have moved all of the practical details of the process from the supplementary information into the main text (‘Detailed process steps’ subsection in Methods). We are confident that all process parameters and materials are now fully described, and that the method could be reproduced by a reader. We appreciate the reviewer’s comment that the process ‘**could provide a transformative impact to … device fabrication**’. What appears to be at issue in this review is whether the process is presented in sufficient detail and is sufficiently optimized to warrant publication. We strongly believe that our revised manuscript is thoroughly detailed and the results are well enough developed to benefit the 2D materials community as they stand, and therefore warrant publication. Our justification lies in (*a*) our extensive optical (reflectance, PL and Raman), topographical, and electrical characterization of transferred material, and (*b*) our introduction and use of two yield metrics (feature and areal yields) which are *in themselves* new to the 2D materials field and whose values represent a major step forwards from what had been described—less quantitatively—before. While the method would undoubtedly need further development before industrial application, we do not think that readiness for industrial application is a necessary prerequisite for publication; the potential to transform research experimentation is more than enough. In the first part of the Methods section (‘Overview and novelty’) we have added text explaining why we think our present feature yields can significantly advance the pace of research.
1. It is still not clear how the presented process is able to selectively exfoliate monolayer structures. Although the authors present a brief justification in the first paragraph of discussion, this discussion is not convincing. Especially, the authors attribute the monolayer generation to the pre-etching of TMDC layers under the gold/resist structures, which could initiate pre-deterministic fracture locations for exfoliating monolayer features. The authors must present additional experimental evidences to show that such a pre-etching	We have added text in the Introduction to clarify current understanding of how the presence of the metal film enables monolayer-selective exfoliation. The monolayer selectivity is provided by the compressive strain in the top 2D layer induced by the metal film which promotes crack propagation between the top two 2D layers. Because of the role of the metal film, in fact ***atomically-precise etching is not required by this technique,*** representing a huge advantage of the method. Rather, sufficient etching is required to expose the edge of the features to *at least* monolayer depth. Therefore, we do not “attribute the monolayer generation to the pre-etching of TMDC layers under the gold/resist structures”. Pre-etching creates the crack initiation locations at the edges of the desired regions, but is not itself responsible for the monolayer nature of exfoliation.

process can reliably or dominantly generate single-layer steps in the source materials. For example, additional HRTEM or SPM results are needed to show the atomic precision for etching TMDC layers. For the TMDC society, the precise etching of TMDC layers is a general challenge. In this manuscript, the authors should not skip the scientific insights and hard evidences for achieving such a critical capability.	We appreciate that this critical distinction may not have been clear in the manuscript, so we have added text at the start of the Methods section to explain this more directly. Some more background on the mechanism is given below for reference: The mechanism of monolayer selectivity has been thoroughly examined—both theoretically and experimentally—in other texts, which we summarize and cite. Specifically, recent work from Sun and co-authors (Sun, *et al.* Theory of thin-film-mediated exfoliation of van der Waals bonded layered materials. *Physical Review Materials*, **2**(9):094004, September 2018) shows that the in-plane compression induced by the epitaxial growth of gold on the chalcogen atoms of the exposed TMDC layer reduces the bond strength per unit area between the top TMDC layer and second TMDC layer. Thus, cracks initiated during stamp removal selectively propagate at this weakest interface, resulting in monolayer exfoliation. A similar approach has been demonstrated experimentally on sulfides and selenides (Desai, S. *et al.* Gold-Mediated Exfoliation of Ultralarge Optoelectronically-Perfect Monolayers. *Advanced Materials* **28**(21), 4053–4058 (2016)), and similar methods have been used to transfer graphene, albeit without monolayer selectivity, using Ni as the epitaxial metal (Kim, J. *et al.* Layer-Resolved Graphene Transfer via Engineered Strain Layers. *Science* **342**, 833–836 (2013)). Furthermore, this understanding is detailed extensively in **Section S2: Theory of metal film assisted exfoliation** in our Supplemental Information.
2. Raman characterizations for to-be-exfoliated TMDC features and as-exfoliated TMDC features should be provided for evaluating if the transfer printing process introduces any critical damage to the TMDC layers.	The to-be-exfoliated TMDC features are multilayer (bulk) in nature. It is unclear what additional information would be gained from Raman spectroscopy of the to-be-exfoliated features which would allow us to compare Raman spectrograms after exfoliation and determine damage extent. We think that the explanation now added at the start of the Methods section (‘Overview and novelty’) will make it clear that the to-be-exfoliated material is bulk and would hence not have comparable Raman characteristics.
3. The electronic characterizations are too primitive. Field-effect mobility, On/Off ratio, and subthreshold swing data should be extracted and presented in a statistical way. In addition, transfer length measurement (TLM) should be performed to evaluate the contact resistances between exfoliated TMDC features and Ni contacts.	The specific purpose of the electrical measurements shown in this manuscript is to provide information on the *spatial consistency* of the transferred material as well as its electrical continuity. We report *ranges* of On/Off ratios in the main text (‘Electrical characterization’, pages 16–17) for both MoS_2 (sample size: 20) and WS_2 (sample size: 6) FETs. We also show the I_D–V_{GS} curves for all of these devices in Figures S7 and S8, enabling the reader to visualize the level of consistency between devices readily. Measurements of contact resistance, subthreshold swing, and mobility would be important for engineering devices with specific applications, but are not central to showing the

	consistency of the material obtained in this first demonstration of the process. We think that the On/Off ratios alone provide a suitable point of comparison with the many TMD devices that have been fabricated by others. In some cases devices shown in other work are electrically characterized more extensively, but usually without any associated reports of material or device yield.
4. The authors mention that the exfoliation selectivity is also associated with Au-S bonding. How can this scheme be applied for other TMDC materials? For example, can selenide-based TMDC features be processed using the similar processing condition? If applicable, the exfoliation results for WSe2 features should be presented.	The Au bonding scheme has also been successfully applied with selenides (see Supplemental Information provided in Desai, S. *et al.* Gold-Mediated Exfoliation of Ultralarge Optoelectronically-Perfect Monolayers. *Advanced Materials*, **28**(21), 4053–4058 (2016)). However, we note that the mechanism identified in Sun, *et al.* Theory of thin-film-mediated exfoliation of van der Waals bonded layered materials. *Physical Review Materials*, **2**(9):094004, September 2018 is very general – all that one needs to do is identify a film that will impose epitaxial strain and can later be etched. Au works well for TMDCs, but other materials may also work well for both TMDCs and other 2D materials. We also note that Shim et al., *Science* 362, pp. 665-670 (2018) use a nickel film to fabricate wafer scale samples of graphene. In the present work we have demonstrated our comprehensive process flow for the transfer of two materials: MoS_2 and WS_2. Certainly we would want to apply the method to other materials in future work, but we think that the present work, as it stands, represents a useful and immediately applicable technique, and we do not think the addition of further materials such as WSe_2 is necessary for publication of the present work.We have added words to the Conclusion to emphasize that we have demonstrated the technique with two materials, and that other materials could be studied in future work.
5. The whole manuscript is not arranged in a standard ACS Nano fashion. Especially, it lacks all detailed descriptions of the experimental conditions and results, which are critical for other researchers to repeat the presented methods.	Our new submission to ACS *Applied Materials and Interfaces* follows the author guidelines for this journal. In the previous submission, detailed descriptions of all experimental and process conditions were included in the Supplemental Information. Specifically, section **S3. Transfer process steps** in our original submission detailed the process steps. We have now moved all of these details to main text to increase ease of reading. Meanwhile, Section **S6. Further electrical characterization** details in full the fabrication of contacts for device measurement, and is referred to directly at the relevant point in the main text where the electrical testing results are described. In contrast with this reviewer, we note that reviewers 1, 3, and 4 all agreed that "*the manuscript give[s] a complete description of the procedures that could be reproduced by others in the field*". The results are described quantitatively, with detailed optical, PL, Raman, AFM and electrical characterization for which full

	methods are given and whose results are all described in detail in the figures and text. Indeed, we think that our extensive presentation and discussion of two yield metrics (feature and areal yield) results in a manuscript that is *richer* in quantitative process data than many contemporary publications in the field.
Reviewer 3	
1. The authors greatly exaggerate the motivation for the approach in the introduction. A few examples are: "Firstly, although single-layer vapor-phase deposition techniques such as chemical vapor deposition are now maturing1,15, the development of processes to deposit one specific 2D material on top of another, while possible16,17, is time-consuming." This is not very convincing, since the procedure proposed by the authors is far more time consuming and requires an excessive number of steps and includes the use of 100 nm of gold – which essentially makes it non-scalable and cost prohibitive.	Growing one wafer of high-electronic-quality MoS_2 monolayers typically requires 26 hours (Kang, K. *et al.* High-mobility three-atom-thick semiconducting films with wafer-scale homogeneity. *Nature* **520**, 656-660 (2015)). This is before subsequent transfer to a substrate, and patterning. We have added a reference to this growth time into the Introduction to emphasize our point. In contrast, our process, which results in patterned monolayers on a target substrate, requires fewer than 10 hours, before any automation. The most time-costly steps are the evaporation (~45 minutes are required for vacuum pump-down), the photolithographic patterning (~1 hour), and the acetone rinse (4 hours). We have added this information to the early part of the Methods section. A detailed accounting of the time required for each process step can be provided upon request. Moreover, the cost of gold is not at all prohibitive. This indicates a lack of understanding of process costs on the part of the reviewer. Evaporating 100 nm of gold over a 12" wafer requires 140 mg of gold, at a total material cost of less than $10. Such a sum is insignificant in the total cost of chip production.
"many applications such as LED displays will demand larger ($\gtrsim 10\ \mu m$) planar junctions between sheets of material" This is certainly true, but the manuscript generally doesn't show homogeneity over any consistent length scale. This is exemplified by the variations in PL and low yield of electrically active devices. With other methods, these yields are far better.	Text has been added to the "Optical characterization of transferred material" section within the results, to emphasize that spatial variation of PL intensity is not indicative of an absence of continuous monolayer material. The visible PL intensities recorded in, e.g., Fig 2b are all within a range that confirms monolayer material to be present; multilayer material would be orders of magnitude dimmer. PL intensity variation may indicate sulfide vacancies that compromise quantum yield. In any case, superacid repair of the material has been demonstrated. In the optical reflectance image in Figure 2a, for example, there are over 100 well defined polygons of WS_2 material. A clear majority of them show material with uniform coloring over >100 µm, which is evidence of continuous monolayer material over these distances. The distribution of the sizes of monolayer regions is detailed in the histograms of Fig 2. For exfoliated material these results are unprecedented. Despite extensive study of the literature we do not know of any other methods with better yields as the reviewer claims. If

	a reviewer can point us to such a method we would of course reference and address it.
"to define the boundaries of, e.g., powerful individual visible light emitters or sensitive detectors requiring dimensions in the tens of microns or larger." I really cannot see how a stamping process could be more efficient than etching. It is a novelty to stamp exact dimensions, but maybe not necessarily useful.	We have strengthened the part of the Introduction that discusses the challenges of vapor phase deposition followed by etching: "Secondly, when a particular layer of a heterostructure needs to be patterned without destroying those underneath—e.g. to enable electrical contact—either extremely high etch selectivity or atomically precise control of etching depth is needed. These requirements are likely to be impractical to achieve because of difficulties in selecting appropriate etchants and inevitable etch-rate spatial nonuniformities." We have also added the following text to the overview of the process ('Overview and novelty' in Methods): "Etching material on the substrate *post-transfer* would not overcome this limitation [sparse transfer when blanket transfer is being attempted]. Patterning the crystal *before* exfoliation, as we do, succeeds in dictating where material will be exfoliated." Our work is premised on the idea that transfer, followed by patterning by etching, is ill-suited to the fabrication of heterostructures. Certainly, forgoing patterning and attempting to remove wafer-scale monolayers—as recently demonstrated on graphene by Shim and co-authors (Shim, J. et al. Controlled crack propagation for atomic precision handling of wafer-scale two-dimensional materials. Science 362, pp. 665-670 (2018))—would result in larger exfoliated areas. However, transferring these large areas on top of existing 2D material patterns, then patterning the transferred material by etching, would almost certainly result in damage to, or destruction of, the portion of the underlaying material exposed to the etchant. This issue significantly restricts the achievable device geometries, most likely only allowing perfectly-overlapping stacks.
2. The process is inherently limited by micro fissures, particulate contamination, strain, exposure to heat (Sulphide vacancy formation) and variable doping. While the authors repeatedly claim feature sizes larger than 100x100 microns, this seems to be unproven by the lack of actual electrical data showing that the features are conducting over this length scale. It is somewhat unlikely to be consistently true for any exfoliation method since the source crystals are not single crystal.	The single-crystal nature of the source only modulates the apparent electron mobility over long distances (since grain boundaries act as defects). A multi-crystal monolayer may still be conducting, as is apparent from CVD sources with sub-micron grain sizes (Zhang, J. *et al.* Scalable Growth of High-Quality Polycrystalline MoS_2 Monolayers on SiO_2 with Tunable Grain Sizes. *ACS Nano* **8**, 6024–6030 (2014)). To the extent that this is a concern, naturally-occurring sources typically have much larger grain sizes than synthetic, including CVD-grown, sources (Zhang *et al.*). The potential for our process, like any exfoliation process, to damage the material is self-evident. However, while we have not yet developed devices that conduct across the entire 100 micron length-scale, we have fabricated many devices at randomly selected locations and found them to be functional. In particular, for the MoS_2 case, all 20 of the 20 tested devices worked. This result implies that the MoS_2 is, indeed,

	contiguous across the fabricated feature size, which is certainly of the order of 100 microns. Therefore, there is no evidence of 'micro fissures' playing a role in the performance of the exfoliated material, as is asserted by the reviewer. We address particulate residues in our response to Reviewer 1, comment 2, explaining that the residues have been found neither to compromise the functioning of any of the FETs tested nor to prevent construction of a bilayer with atomically close contact. This process is inherently low-temperature: the highest temperature reached during the transfer process is 160 °C, far lower than, *e.g.*, CVD. We are not sure at what stage the reviewer believes that 'variable doping' occurs; doping is not carried out in this process.
3. Low yield - In Supplemental S7, it is mentioned that only 20 monolayer devices with functional MoS2 channels were measured. This number really has to be improved if the authors wish to publish outside of a specialized journal.	We tested 20 devices at randomly selected locations within established monolayer regions of MoS_2 to provide a basis for analyzing variability of their characteristics. Therefore, the relevant device yield metric is the *fraction of tested devices that were functional*. *Every single one* (20/20) of the tested MoS_2 devices was functional. The reviewer may be under the impression that we tested hundreds of devices and found 20 that worked – that is not the case; our entire sample of MoS_2 devices functioned as FETs. We have amended the Methods text on electrical testing to make this clearer.
4. AFM height measurements between silicon oxide (and most non-van der Waals materials) are not accurate and should probably not be utilized as evidence of monolayer. This has been known for decades, but is mentioned even in the very first papers on graphene in 2004-2005. With adhesive force (e.g. the phase data in Figure S9.) so dramatically different between the layers, tapping mode will never give accurate results. It is fine to use the measurement as a rough estimate of layer numbers, but measurement of such high precision (0.563 nm) is both impossible with such a dirty substrate, and also misleading. The measurement should be done with respect to an hBN or other clean van der Waals material as a substrate.	We originally omitted AFM data from the manuscript for this very reason. However, in response to an editorial request from *ACS Nano*, we included AFM data to supplement the findings of optical, photoluminescence and Raman data, even though PL alone gives a more robust indication of the monolayer nature of the material. Nevertheless, other authors (*e.g.* Dumcenco, D. *et al.* Large-Area Epitaxial Monolayer MoS_2. *ACS Nano* **9**, 4611–4620 (2015)) do use AFM to extract the height of monolayer MoS_2 on an amorphous substrate. Notably, the work of Dumcenco *et al.* shows a raised region at the edge of the MoS_2 flake in Figure 1d, as we observe in our work. We have amended: "Raman spectroscopy **and atomic force microscopy** confirm the single-layer nature of regions identified as monolayer by optical assessment and PL (supplementary Figs. S5–S6 and S8–S9)." to "Raman spectroscopy (supporting section S5 and Figs. S5–S6 and S8) further confirms the single-layer nature of regions that had already been identified as such by both optical reflectance and PL." and have placed the text

	"Atomic force microscopy (AFM) measurements of transferred material were also performed (supplementary Figs. S9–S11 and Section S9)." at the start of a new section of the Results and Discussion entitled "Atomic force microscopy and surface residues". These changes reflect the fact that we do *not* use AFM as to determine whether material is monolayer. We have also removed from figures S9 and S10 the dimensional measurements that showed unwarranted precision.
5. PL data is also misleading. The use of super acid is used to counter chalcogenide vacancies. Significantly reduced improvements in PL efficiency (single digit improvement at best, or even unity) are found in flakes placed onto hBN substrates and not subject to air annealing. The huge improvements claimed by the authors are a sign that the transfer procedure is removing chalcogenide atoms from the flakes, which need to be healed afterwards via super acid.	We are not sure how this reviewer believes the presented results are misleading. We present non-superacid-treated PL measurements alongside PL measurements from the same samples treated in superacid. It is possible the bonding and debonding of gold to sulfur atoms results in their removal. Moreover, the source flakes are themselves imperfect and contain chalcogen vacancies.
6. If claims are to be made within the text regarding the usefulness of the method – those claims should be demonstrated or removed. Specifically, most of page 7 seems to be listing future experiments or claims such as "exceptionally large-area transfer" – which the manuscript most certainly does not show.	We cite results presented in the present text (areas > 10^4 μm^2) to justify our claim of large-area transfer on page 7. We have removed the word "exceptionally" to avoid any subjective assessment of the merit of this demonstrated area.
Reviewer 4	
The work presented by the authors addresses an important question: the efficient preparation of large exfoliated 2D TMDC crystals assisted by gold. The ability of gold to enable the exfoliation of large area TMDC monolayers was first demonstrated by Magda et al., then further developed by other groups. The present work goes along this line; it also employs a gold sacrifice layer to exfoliate 2D TMDC crystals, so conceptually it doesn't bring much novelty. The main result of this work is that compared to a continuous	We appreciate the reviewer's comment about the importance of efficient preparation of exfoliated TMDC monolayer regions. We would like to clarify that our manuscript is not merely presenting a yield increase of a known process, but is describing an *entirely new* processing flow that accomplishes control over shape and position in a way that has not been seen before. The yield of the resulting monolayer regions is a closely related and very important issue, but yield is not the main source of the novelty of the manuscript. We present here a method for transferring patterned monolayers over large areas – this has not previously been reported using gold-assisted exfoliation (or indeed otherwise).

gold sacrifice layer, a patterned gold layer enhances the exfoliation yield. However, **the yield increase alone is not substantial enough** to justify the publication in a high impact journal.	Therefore, we do believe that our work is a significant advance over the existing understanding. We are introducing a nanomanufacturing process rooted in mechanical exfoliation. Until very recently, this was not considered to be viable, despite the prior art of Magda *et al.* and the nearly contemporaneous developments of Desai *et al.* Now, we are at the point where we can have serious discussions about the yield of our nanomanufacturing process. So, this work demonstrates an entirely new method for producing patterned monolayers. The high yield merely reinforces the value of this new method.
Due to the incremental nature of the results , it would be more suitable for a more specialized journal. **The spatially precise transfer claim would be really useful if the monolayer yield would be higher. This way it only can tell us for sure at which locations there will be no TMDC layer.** This approach can be achieved by using previously demonstrated methods where large, up to cm2 area single layers can be exfoliated, then transferred and patterned into the desired structures.	As noted in our response to Reviewer 3, our work is premised on the idea that transfer, followed by patterning, is ill-suited to the fabrication of heterostructures. As we wrote to Reviewer 3: Certainly, forgoing patterning and attempting to remove wafer-scale monolayers (as recently demonstrated on graphene by Shim and co-authors (Shim, J. *et al.* Controlled crack propagation for atomic precision handling of wafer-scale two-dimensional materials. *Science* 326 , 665 (2018)) would result in larger exfoliated areas. However, transferring these large areas atop existing 2D material patterns, and then patterning the just-transferred large-area layer, could result in damage to underlaying layers. Such an approach significantly restricts the achievable device geometries, only allowing perfectly-overlapping stacks. Our method is, at the very least, another useful weapon in the arsenal of device designers.
In conclusion, I think that **the advancement brought by the present approach would only be significant enough if the yield could be increased above 80-90%**. Otherwise, neither the novelty, nor the technical progress is significant enough to warrant top level publication.	No previously reported stamp exfoliation method assesses yield in any meaningful way. Patterned exfoliation methods for 2D materials have not before resulted in monolayer transfer. The only comparable methods are large-area-transfer followed by patterning, which is unsuitable for heterostructure fabrication (see above comment). Of course, we hope to improve the yield of this process moving forward. Nonetheless, we think this is an important first step and 80-90% yield seems rather arbitrary and unreasonably high when there is no existing benchmark for yield in any work in the field. The novelty lies in the new capabilities offered by the method, which we believe is sufficiently novel to warrant publication, even in the absence of production-quality yield.